NATIONAL ADVISORY COMMITTEE FOR AERONAUTICS

TECHNICAL NOTE 3649

STATIC LONGITUDINAL AND LATERAL STABILITY CHARACTERISTICS AT LOW SPEED OF UNSWEPT-MIDWING MODELS HAVING WINGS WITH AN ASPECT RATIO OF 2, 4, OR 6

By Walter D. Wolhart and David F. Thomas, Jr.

Langley Aeronautical Laboratory
Langley Field, Va.

Washington
May 1956

NATIONAL ADVISORY COMMITTEE FOR AERONAUTIC

TECHNICAL NOTE 3649

STATIC LONGITUDINAL AND LATERAL STABILITY CHARACTERISTICS AT LOW SPEED OF UNSWEPT-MIDWING MODELS HAVING WINGS WITH AN ASPECT RATIO OF 2, 4, OR 6

By Walter D. Wolhart and David F. Thomas, Jr.

SUMMARY

A systematic investigation was made in the Langley stability tunnel to determine the effects of the various components and combinations of components on the static longitudinal and lateral stability characteristics at low speed of unswept-midwing models having wings with an aspect ratio of 2, 4, or 6 through an angle-of-attack range from -4° to 32°. Also included are the effects of large angles of sideslip at several angles of attack for some of the components and combinations of components.

The results of this investigation have indicated that, at low and moderate angles of attack, decreasing wing aspect ratio decreases the tail contribution to longitudinal stability. Near the angle of maximum lift for the wing-alone configuration, there is a pronounced increase in longitudinal stability for all configurations involving the wing for all wing aspect ratios.

For the complete model, changes in wing aspect ratio generally had little effect on the tail contribution to directional stability throughout the angle-of-attack range investigated. The most noticeable effect of wing aspect ratio on the lateral stability characteristics occurred for configurations involving the aspect-ratio-2 wing-fuselage combination. These configurations showed abrupt variations in the sideslip derivatives or hysteresis occurring at small angles of sideslip for angles of attack of about 20° and 26°, respectively.

A large decrease exists in the vertical-horizontal tail contribution to directional stability at moderate and high angles of attack because of wing-fuselage interference at the tail which is counteracted by a stable shift in the directional stability of all wing-fuselage combinations. This combination of effects results in all complete-model configurations being directionally stable throughout the angle-of-attack range investigated.

INTRODUCTION

In general, the stability characteristics of midwing or near-midwing airplanes can be estimated with good accuracy at low angles of attack by various theoretical and empirical methods such as those presented in reference 1. The results, however, at moderate and high angles of attack are oftentimes unreliable because of the unpredictable interference effects of the various components.

Considerable information is available on the influence of the wing, fuselage, and tail geometry on the static stability characteristics of high-aspect-ratio unswept-wing configurations (for example, refs. 2 to 4). More recent information on unswept-wing models is presented in references 5 to 8, for example. However, there is little information of a systematic nature on the effects of wing aspect ratio for complete models.

This paper presents the results of a systematic investigation to determine the effects of the various components and combinations of components on the static stability characteristics at low speed of unswept-midwing models having wings with an aspect ratio of 2, 4, or 6 through an angle-of-attack range from -4° to 32°. Also included are data for large angles of sideslip at several angles of attack for various components and combinations of components.

SYMBOLS

The data presented herein are in the form of standard coefficients of forces and moments which are referred to the stability system of axes with the origin at the projection on the plane of symmetry of the calculated aerodynamic center of the wing. Positive directions of forces, moments, and angular displacements are shown in figure 1. The coefficients and symbols are defined as follows:

A	aspect ratio, b^2/S
b	span, ft
S	surface area, sq ft
c	local chord parallel to plane of symmetry, ft
$\bar{c}$	mean aerodynamic chord, $\frac{2}{S}\int_0^{b/2} c^2 dy$, ft

y spanwise distance measured from and perpendicular to plane of symmetry, ft

l tail length, distance measured parallel to fuselage center line from mounting point to $\bar{c}/4$ of the tail, ft

q dynamic pressure, $\rho V^2/2$, lb/sq ft

ρ mass density of air, slugs/cu ft

V free-stream velocity, ft/sec

R ordinate of circular fuselage, in.

x longitudinal distance from fuselage nose measured parallel to fuselage reference line, in.

α angle of attack, deg

β angle of sideslip, deg

C_L lift coefficient, $\frac{\text{Lift}}{qS_w}$

C_D drag coefficient, $\frac{\text{Drag}}{qS_w}$

C_Y lateral-force coefficient, $\frac{\text{Lateral force}}{qS_w}$

C_m pitching-moment coefficient, $\frac{\text{Pitching moment}}{qS_w\bar{c}_w}$

C_l rolling-moment coefficient, $\frac{\text{Rolling moment}}{qS_wb_w}$

C_n yawing-moment coefficient, $\frac{\text{Yawing moment}}{qS_wb_w}$

$C_{Y_\beta} = \frac{\partial C_Y}{\partial \beta}$ per degree

$C_{n_\beta} = \frac{\partial C_n}{\partial \beta}$ per degree

$C_{l_\beta} = \frac{\partial C_l}{\partial \beta}$ per degree

Subscripts:

w	wing
VH	contribution of the vertical-horizontal tail assembly to various force and moment coefficients
t	tip
r	root
max	maximum

Model component designations:

W	wing alone
F	fuselage alone
VH	vertical-horizontal tail combination, always tested as a unit (tail alone)
WF	wing-fuselage combination
WVH	wing-tail combination
FVH	fuselage-tail combination
WFVH	wing-fuselage-tail combination (complete model)

Nomenclature used to denote configurations involved in method of subtracting data of various configurations to obtain the contribution of the vertical-horizontal tail assembly to the various force and moment coefficients.

FVH-F	fuselage-tail combination minus fuselage alone
WVH-W	wing-tail combination minus wing alone
WFVH-WF	complete model minus wing-fuselage combination

APPARATUS AND MODELS

This investigation was made in the 6-foot-diameter test section of the Langley stability tunnel. The models were mounted on a single strut support which was in turn fastened to a conventional six-component balance system.

The models used in this investigation were constructed primarily of laminated mahogany and consisted of three unswept wings with an aspect ratio of 2, 4, or 6, a fuselage with a fineness ratio of 7.5, and unswept vertical and horizontal tails with aspect ratios of 2 and 4, respectively. In general, the models were designed to permit testing of the individual components as well as various combinations of the components. The only exceptions were the horizontal and vertical tails which were not separable and were always tested as a unit. For the wing-tail configurations, the tails were mounted at the appropriate tail length on a steel tube of small diameter which was in turn fastened to the wing. The isolated tails were mounted on the same tube which was then attached to the model support strut. Geometric characteristics of the various components are given in figures 2 and 3 and table I. The coordinates of the fuselage are given in table II. Photographs of two model configurations are presented in figure 4.

TESTS AND CORRECTIONS

All the tests were made at a dynamic pressure of 24.9 pounds per square foot which corresponds to a Mach number of 0.13. The Reynolds numbers based on the mean aerodynamic chord of the various wings were 1.02×10^6 for the aspect-ratio-2 wing, 0.72×10^6 for the aspect-ratio-4 wing, and 0.59×10^6 for the aspect-ratio-6 wing. The static longitudinal and lateral stability characteristics were obtained for an angle-of-attack range from approximately -4° to 32° from tests made at angles of sideslip of 0° and $\pm 5^\circ$. In addition, several configurations were tested through a sideslip range from -20° to 20° for several angles of attack.

Approximate jet-boundary corrections were applied to the angle of attack and drag coefficients by the methods of reference 9. Horizontal-tail-on pitching-moment coefficients were corrected for the effects of the jet boundaries by the methods of reference 10. These data are not corrected for the effects of the support strut or blockage.

PRESENTATION OF RESULTS

The basic static longitudinal-stability data, which show the variation of C_L, C_D, and C_m with α for the various components and combinations of components, are presented in figures 5 and 6. The effects of the various components on the tail contribution to C_L and C_m are presented in figures 7 and 8, respectively. The effects of wing aspect ratio on the variation of $C_{m,VH} \times \bar{c}_w/l$ with α are presented in figure 9. Examples of the effect of sideslip angle on the static longitudinal stability characteristics of various configurations at several angles of attack are presented in figures 10 to 13.

Examples of the variation of C_Y, C_n, and C_l with β for various configurations at several angles of attack are presented in figures 14 to 18. The basic static lateral-stability data, which show the variation of C_{Y_β}, C_{n_β}, and C_{l_β} with α for the various components and combinations of components, are presented in figures 19 and 20. The effects of the various components on the tail contribution to C_{Y_β}, C_{n_β}, and C_{l_β} are presented in figures 21 to 23. The effects of wing aspect ratio on the variation of $C_{n_\beta,VH} \times b_w/l$ with α are presented in figure 24.

DISCUSSION

In general, the discussion of the results of this investigation will be confined to pitching-moment and directional stability characteristics. It should be kept in mind throughout this discussion that comparing moment coefficients for similar configurations, where wing aspect ratio is the only variable, can be somewhat misleading since the coefficients are based on geometric characteristics of the wing and, therefore, are not based on a common length. The effect of changing the basis of the moment coefficients is illustrated in figures 6 and 20 for the wing-off configuration. The force coefficients, however, are directly comparable since the wing area remained constant for all wing aspect ratios.

Static Longitudinal Stability Characteristics

Basic static longitudinal stability characteristics.- The basic static longitudinal stability characteristics are presented in figures 5 and 6 for wing-on and wing-off configurations, respectively. These data show that all complete-model configurations are unstable at low angles of attack for the present center-of-gravity location. An examination of wing-on and wing-off data shows, as might be expected, that this instability is largely due to the unstable contribution of the fuselage and a reduction in the horizontal-tail contribution to pitching-moment coefficient $C_{m,VH}$ when the tail acts in the presence of the wing. At angles of attack approaching $C_{L,max}$ for the wing-alone configuration, there is a pronounced increase in longitudinal stability for all configurations involving the wing for all wing aspect ratios because of a rearward shift in center of pressure on the wing. Apparently, the NACA 65A008 airfoil sections used on these wings exhibit the thin-airfoil type of stall (a stall that is preceded by flow separation at the leading edge with reattachment at a point which moves progressively rearward with increasing angle of attack), noted in reference 11, and a subsequent rearward shift in center of pressure. The fact that this increase in stability continues over a larger angle-of-attack range for tail-on configurations is attributed to an increase in $C_{m,VH}$ as the center of the wing wake moves farther above the tail with increasing angle of attack. A more detailed discussion of how $C_{m,VH}$ is influenced by interference from the various components is given in the following section.

Tail contributions.- The effects of interference from the various components on the contribution of the vertical-horizontal tail combination to lift and pitching-moment coefficients are presented in figures 7 and 8, respectively, which show the variation of $C_{L,VH}$ and $C_{m,VH}$ with α. These data show that the wing has the most marked effect on the tail contribution to pitching moment and decreases $C_{m,VH}$ appreciably at both low and moderate angles of attack because of either downwash or decreased dynamic pressure or both in the region of the tails. This condition is further aggravated for the tails in the presence of the wing-fuselage combination, although the fuselage itself had little effect. The larger decrease in $C_{m,VH}$ for the tails in the presence of the wing-fuselage combination as compared with that for the wing alone is attributed to increased downwash associated with the increased lift-curve slope (fig. 5) of the wing-fuselage combination. At high angles of attack there is an increase in $C_{m,VH}$ as the center of the wing wake moves farther above the tail and $C_{m,VH}$ approaches that of the wing-off case.

As mentioned previously, the effects of wing aspect ratio on pitching moment, when presented in coefficient form, are somewhat obscure because of the decrease in $\bar{c}_w$ with increasing aspect ratio; therefore, figure 9 has been prepared and shows the variation of $C_{m,VH} \times \bar{c}_w/l$ with α. Multiplying $C_{m,VH}$ by $\bar{c}_w/l$ gives a pitching-moment coefficient based on the tail length l which was the same for all configurations. These data show a large decrease in the tail contribution to pitching moment for the tail in the presence of the wing either with or without a fuselage because of either downwash or decreased dynamic pressure or both. As might be expected, decreasing wing aspect ratio decreases the tail contribution to pitching moment since downwash varies inversely with wing aspect ratio.

Variation of C_L and C_m with β.- The variation of C_L and C_m with β at several angles of attack for the complete model employing the aspect-ratio-2 wing plus several of its components is shown in figures 10 to 12. Data were also obtained for the complete model employing the aspect-ratio-4 wing and these data are presented in figure 13. These data show that C_L and C_m remain essentially constant for angles of sideslip up to about 10° at angles of attack of about 0° and 10° for the complete model employing either the aspect-ratio-2 or the aspect-ratio-4 wing. However, at angles of attack of about 20° and 26°, sideslipping the complete model in either direction from $\beta = 0^\circ$ results in a positive increment in pitching-moment coefficient with increasing angle of sideslip with either the aspect-ratio-2 or aspect-ratio-4 wing.

In general, adding the tails to the aspect-ratio-2 wing-fuselage combination or wing-alone configuration has little effect on the variation of C_m with β at angles of attack of about 20° and 26°. (Compare figs. 10(a) with 10(b) and 11(a) with 11(b).) The main exception is the wing-tail configuration at an angle of attack of about 26° which shows a negative increment in C_m when the model is sideslipped from $\beta = 0^\circ$ for angles of sideslip up to about $\pm 10^\circ$. For wing-off configurations (fig. 12), sideslipping the model had little effect on C_m for sideslip angles up to about $\pm 10^\circ$. In general, then, it appears that the positive increment in C_m when the complete model is sideslipped from $\beta = 0^\circ$ is due in a large part to a forward shift in center of pressure on the wing-fuselage combination.

Static Lateral Stability Characteristics

Variation of C_Y, C_n, and C_l with β.- Before discussing the static lateral stability characteristics as determined from $\beta = \pm 5^\circ$, some consideration will be given to the variation of C_Y, C_n, and C_l with β at several angles of attack. Data were obtained for the complete model employing the aspect-ratio-2 wing plus the various components and are presented in figures 14 to 17. Data were also obtained for the complete model employing the aspect-ratio-4 wing and these data are presented in figure 18.

These data show that the curves of C_Y, C_n, and C_l plotted against β are reasonably linear for angles of sideslip up to about $\beta = \pm 10^\circ$ for angles of attack of approximately 0° and 10° for the complete model employing either an aspect-ratio-2 or aspect-ratio-4 wing. At angles of attack of approximately 20° and 26°, however, some rather sharp breaks in the curves occur for the complete model with the aspect-ratio-2 wing at small sideslip angles, and these data show the aerodynamic hysteresis noted in reference 7. The aerodynamic hysteresis is most noticeable at $\alpha = 26^\circ$ and is characterized by a discontinuity in the curves of C_Y, C_n, and C_l with β. The breaks occur at positive angles of sideslip when the sideslip angle is varied from negative to positive, and when the sideslip angle is varied from positive to negative the converse is true. The curves have been faired to show breaks occurring at the angle of sideslip at which large changes in loading on the model take place as noted by visual observation of the balance indicators. It should be pointed out that no evidence of hysteresis was found in the static longitudinal stability characteristics (figs. 10 to 13).

The reason as to why hysteresis shows up in the lateral stability characteristics is not known, and it appears that flow studies or pressure-distribution tests are necessary in order to establish the nature of the flow over the model. However, from an examination of the results for the various components and combinations of components for the aspect-ratio-2 model (figs. 14 to 17), it becomes evident that the hysteresis is due to an aerodynamic phenomenon associated with the wing-fuselage combination. Some nonlinearities were noted in the data near $\beta = 0^\circ$ for the wing alone or the wing-tail configuration at an angle of attack of about 20°, but there was no hysteresis for these configurations. At the present time, about all that can be said by way of explanation of the hysteresis is that once a definite loading has been established on the wing-fuselage combination, the combination tends to retain the loading even though the sideslip angle is reversed.

The hysteresis, although occurring at angles of attack which are beyond the normal flight range of airplanes, may become important during maneuvers at high altitudes, especially for missiles. It is expected that the hysteresis might be affected appreciably by increasing the Reynolds number, although a check at the highest Reynolds number attainable (1.61×10^6) showed no effect.

Since hysteresis was not obtained with the aspect-ratio-4 complete model (fig. 18), this effect is probably confined to relatively low-aspect-ratio wings. However, as noted in reference 4, the location of the wing-fuselage juncture, which changed with changes in wing aspect ratio, can influence the loading on the center section of the wing appreciably. In addition, changing the shape of the fuselage in the vicinity of the wing by adding closed horizontal ducts to the aspect-ratio-2 complete-model configuration eliminated the hysteresis as shown in reference 7.

Basic static lateral stability characteristics.- The basic static lateral stability derivatives C_{Y_β}, C_{n_β}, and C_{l_β}, plotted against angle of attack, are presented in figures 19 and 20 for wing-on and wing-off configurations, respectively. Since there is considerable uncertainty about the slopes for configurations involving the aspect-ratio-2 wing for angles of attack above about 20° because of the nonlinear variation of C_Y, C_n, and C_l with β near $\beta = 0^\circ$, resort has been made to the use of a dotted-line fairing in order to distinguish this range. Although no extended sideslip data are available for angles of attack between about 10° and 20°, it should be pointed out that the curves of C_Y, C_n, and C_l plotted against β may also be nonlinear for angles of attack somewhat less than 20°.

A comparison of results for tail-on and tail-off configurations shows that a large decrease exists in the vertical-horizontal tail contribution to directional stability at moderate and high angles of attack when the tails act in the presence of the wing or wing-fuselage combination. In approximately the same angle-of-attack range there is a stable shift in the directional stability of all wing-alone or wing-fuselage configurations. These two effects tend to cancel one another and result in all wing-tail or complete-model configurations being directionally stable throughout the angle-of-attack range investigated.

Breaks in the force and moment curves for wing-on configurations generally occur at progressively lower angles of attack with increasing wing aspect ratio as shown in figure 19. These breaks correspond to breaks in the lift and pitching-moment curves as shown in figure 5 and are attributed to flow separation on the wing. The effective dihedral parameter C_{l_β} becomes increasingly negative for wing-on configurations

at the angle of attack corresponding to these breaks. The vertical-horizontal tail combination contributes a large negative increment to C_{l_β} near $\alpha = 0^\circ$, but has little effect at moderate and high angles of attack compared with that of the wing contribution.

Tail contributions.- The contribution of the vertical-horizontal tail combination to the sideslip derivatives is presented in figures 21 to 23. The tail-alone contribution to the directional-stability parameter $C_{n_{\beta,VH}}$ was essentially constant throughout the angle-of-attack range and possibly increased slightly for angles of attack between 8° and 24° as shown in figure 22. The fuselage had little effect on $C_{n_{\beta,VH}}$ throughout the angle-of-attack range investigated.

The tail contribution to directional stability was increased slightly for all wing-tail configurations for angles of attack up to the angle at which flow separation occurs on the wing. Flow separation from the wing is indicated by a reduction in lift-curve slope of the wing alone as well as by breaks in the other force and moment curves. At high angles of attack, the wing interference at the tail was adverse and reduced $C_{n_{\beta,VH}}$ by as much as 50 percent of the value at $\alpha = 0^\circ$.

In general, the tail contribution to C_{n_β} for the complete model is comparable with that for the fuselage-tail combination for angles of attack up to the angle at which flow separation occurs on the wing. Apparently, mutual interference of the wing-fuselage combination decreases or eliminates the favorable interference noted for the wing-tail configuration. The reason as to why the wing-tail configuration results in favorable interference is not known, although the lack of interference for the complete model is in agreement with the theoretical investigation of reference 12. Reference 12 shows that, when the wing is placed in a high or low position on the fuselage, a large spanwise pressure gradient is produced on the sideslipped wing which will induce sidewash at the tail. This static-pressure gradient is due to the antisymmetrical loading induced on the wing by the fuselage and results in adverse and favorable sidewash at the tail for high- and low-wing arrangements, respectively. For midwing arrangements, such as those used in the present investigation, this antisymmetrical loading does not exist and no sidewash is produced. At high angles of attack, adverse interference at the tail due to the wing accounts for about 50 percent of the reduction in tail effectiveness for the complete model with the exception of the aspect-ratio-2 complete model. There are some inconsistencies for configurations employing the aspect-ratio-2 wing, but as mentioned previously, there is considerable uncertainty in these data at high angles of attack because of aerodynamic hysteresis.

A direct measure of how the tail contribution to directional stability is affected by changes in wing aspect ratio is provided in figure 24 which shows the variation of $C_{n_{\beta,VH}} \times b_w/l$ with α. This figure provides a comparison between wing-on and wing-off tail contributions both with and without the fuselage. As mentioned previously, without the fuselage the wing increases the tail contribution to directional stability slightly for angles of attack up to the angle at which flow separation occurs on the wing. The increase is greatest and extends to highest angles of attack for the aspect-ratio-2 wing. Although one might expect a systematic effect of wing aspect ratio, this is not the case herein and the aspect-ratio-6 wing shows a greater increase than the aspect-ratio-4 wing. At high angles of attack, the effects of wing aspect ratio are inconsistent and small in comparison with the effect of angle of attack.

The tail contribution to directional stability for the complete model generally decreases with increasing wing aspect ratio in the angle-of-attack range from approximately 0° to the angle of attack at which flow separation occurs on the wing. The effects shown are small, however, and the results are roughly comparable with those for the tail in the presence of the fuselage. At higher angles of attack, there is a rapid decrease in tail effectiveness for the complete model for all wing aspect ratios, as was the case for the wing-tail configuration. In general, the effects of changes in wing aspect ratio are small in comparison with the effects of angle of attack. Some inconsistencies exist for configurations employing the aspect-ratio-2 wing above about $\alpha = 20^\circ$; but as mentioned before, there is considerable uncertainity in these data because of aerodynamic hysteresis.

CONCLUSIONS

The results of a wind-tunnel investigation to determine the static longitudinal and lateral stability characteristics at low speed of unswept-midwing models having wings with an aspect ratio of 2, 4, or 6 through an angle-of-attack range from -4° to 32° indicate the following conclusions:

1. At low and moderate angles of attack, decreasing wing aspect ratio decreases the tail contribution to longitudinal stability. Near the angle of maximum lift for the wing-alone configuration, there is a pronounced increase in longitudinal stability for all configurations involving the wing for all wing aspect ratios.

2. For the complete model, changes in wing aspect ratio generally had little effect on the tail contribution to directional stability throughout the angle-of-attack range investigated. The most noticeable effect of wing aspect ratio on the lateral stability characteristics occurred for configurations involving the aspect-ratio-2 wing-fuselage combination. These configurations showed abrupt variations in the sideslip derivatives or hysteresis occurring at small angles of sideslip for angles of attack of about 20° and 26°, respectively.

3. A large decrease exists in the vertical-horizontal tail contribution to directional stability at moderate and high angles of attack because of wing-fuselage interference at the tail which is counteracted by a stable shift in the directional stability of all wing-fuselage combinations. This combination of effects results in all complete-model configurations being directionally stable throughout the angle-of-attack range investigated.

Langley Aeronautical Laboratory,
National Advisory Committee for Aeronautics,
Langley Field, Va., February 1, 1955.

REFERENCES

1. Campbell, John P., and McKinney, Marion O.: Summary of Methods for Calculating Dynamic Lateral Stability and Response and for Estimating Lateral Stability Derivatives. NACA Rep. 1098, 1952. (Supersedes NACA TN 2409.)

2. House, Rufus O., and Wallace, Arthur R.: Wind-Tunnel Investigation of Effect of Interference on Lateral-Stability Characteristics of Four NACA 23012 Wings, an Elliptical and a Circular Fuselage, and Vertical Fins. NACA Rep. 705, 1941.

3. Recant, Isidore G., and Wallace, Arthur R.: Wind-Tunnel Investigation of the Effect of Vertical Position of the Wing on the Side Flow in the Region of the Vertical Tail. NACA TN 804, 1941.

4. Jacobs, Eastman N., and Ward, Kenneth E.: Interference of Wing and Fuselage From Tests of 209 Combinations in the N.A.C.A. Variable-Density Tunnel. NACA Rep. 540, 1935.

5. Goodman, Alex: Effects of Wing Position and Horizontal-Tail Position on the Static Stability Characteristics of Models With Unswept and 45° Sweptback Surfaces With Some Reference to Mutual Interference. NACA TN 2504, 1951.

6. Letko, William, and Riley, Donald R.: Effect of an Unswept Wing on the Contribution of Unswept-Tail Configurations to the Low-Speed Static- and Rolling-Stability Derivatives of a Midwing Airplane Model. NACA TN 2175, 1950.

7. Jaquet, Byron M., and Williams, James L.: Wind-Tunnel Investigation at Low Speed of Effect of Size and Position of Closed Air Ducts on Static Longitudinal and Static Lateral Stability Characteristics of Unswept-Midwing Models Having Wings of Aspect Ratio 2, 4, and 6. NACA TN 3481, 1955.

8. Letko, William, and Williams, James L.: Experimental Investigation at Low Speed of Effects of Fuselage Cross Section on Static Longitudinal and Lateral Stability Characteristics of Models Having 0° and 45° Sweptback Surfaces. NACA TN 3551, 1955.

9. Silverstein, Abe, and White, James A.: Wind-Tunnel Interference With Particular Reference to Off-Center Positions of the Wing and to the Downwash at the Tail. NACA Rep. 547, 1936.

10. Gillis, Clarence L., Polhamus, Edward C., and Gray, Joseph L., Jr.: Charts for Determining Jet-Boundary Corrections for Complete Models in 7- by 10-Foot Closed Rectangular Wind Tunnels. NACA WR L-123, 1945. (Formerly NACA ARR L5G31.)

11. McCullough, George B., and Gault, Donald E.: Examples of Three Representative Types of Airfoil-Section Stall at Low Speed. NACA TN 2502, 1951.

12. Schlichting, H.: Aerodynamics of the Mutual Influence of Aircraft Parts (Interference). Library Translation No. 275, British R.A.E., Oct. 1948.

TABLE I.- GEOMETRIC CHARACTERISTICS OF MODELS

Fuselage:			
Length, ft			3.75
Fineness ratio			7.50
Wings:			
Aspect ratio	2	4	6
Quarter-chord sweep angle, deg	0	0	0
Dihedral angle, deg	0	0	0
Twist, deg	0	0	0
Incidence, deg	0	0	0
NACA airfoil section	65A008	65A008	65A008
Area, sq ft	2.250	2.250	2.250
Span, ft	2.122	3.000	3.675
Mean aerodynamic chord, ft	1.083	0.766	0.625
Root chord, ft	1.326	0.938	0.765
Tip chord, ft	0.795	0.563	0.459
Taper ratio	0.6	0.6	0.6
Vertical tail:			
Aspect ratio			2.6
Quarter-chord sweep angle, deg			0
NACA airfoil section			65A008
Area, sq ft			0.338
Span from fuselage center line, ft			0.825
Mean aerodynamic chord, ft			0.418
Root chord, ft			0.512
Taper ratio			0.6
Ratio of tail area to wing area			0.150
Tail length, distance measured parallel to fuselage center line from mounting point to $\bar{c}/4$ of the tail, ft			1.392
Horizontal tail:			
Aspect ratio			4.0
Quarter-chord sweep angle, deg			0
Incidence, deg			0
NACA airfoil section			65A008
Area, sq ft			0.450
Span, ft			1.342
Mean aerodynamic chord, ft			0.343
Root chord, ft			0.419
Taper ratio			0.6
Ratio of tail area to wing area			0.200
Tail length, distance measured parallel to fuselage center line from mounting point to $\bar{c}/4$ of the tail, ft			1.392

TABLE II.- COORDINATES OF THE

CIRCULAR-CROSS-SECTION FUSELAGE

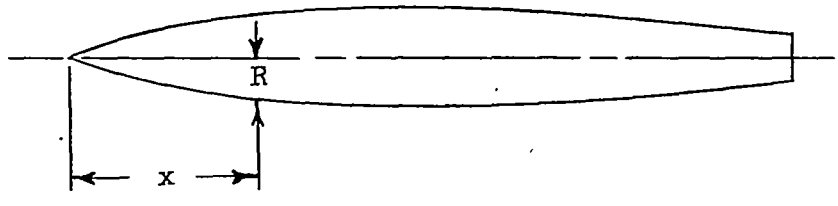

x, in.	R, in.
0	0
2	.64
4	1.20
6	1.68
8	2.09
10	2.42
12	2.67
14	2.85
16	2.96
18	3.00
20	2.99
22	2.97
24	2.93
26	2.87
28	2.79
30	2.70
32	2.60
34	2.47
36	2.33
38	2.18
40	2.01
42	1.82
44	1.61
45	1.50

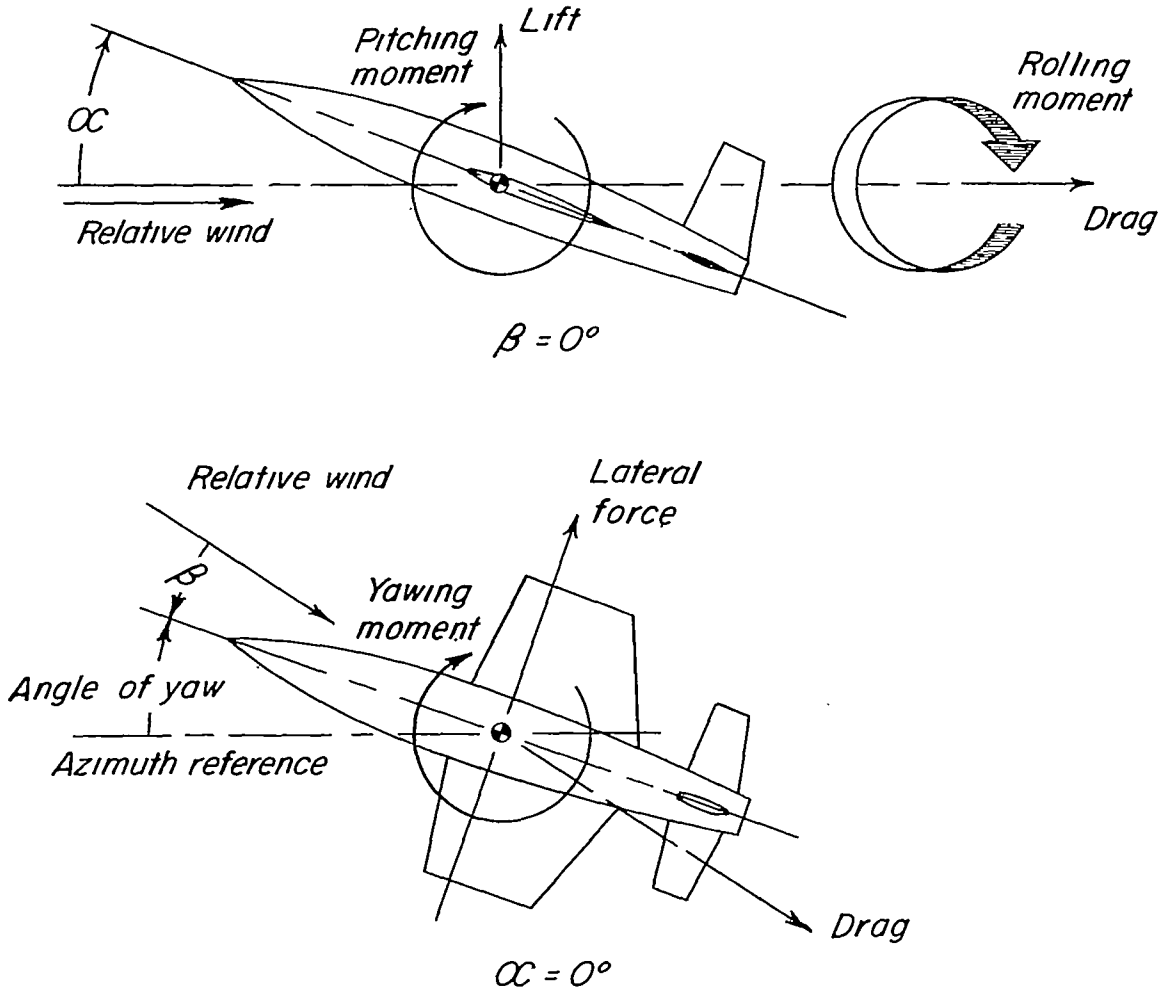

Figure 1.- Stability system of axes used. Arrows indicate positive direction of forces, moments, and angular displacements.

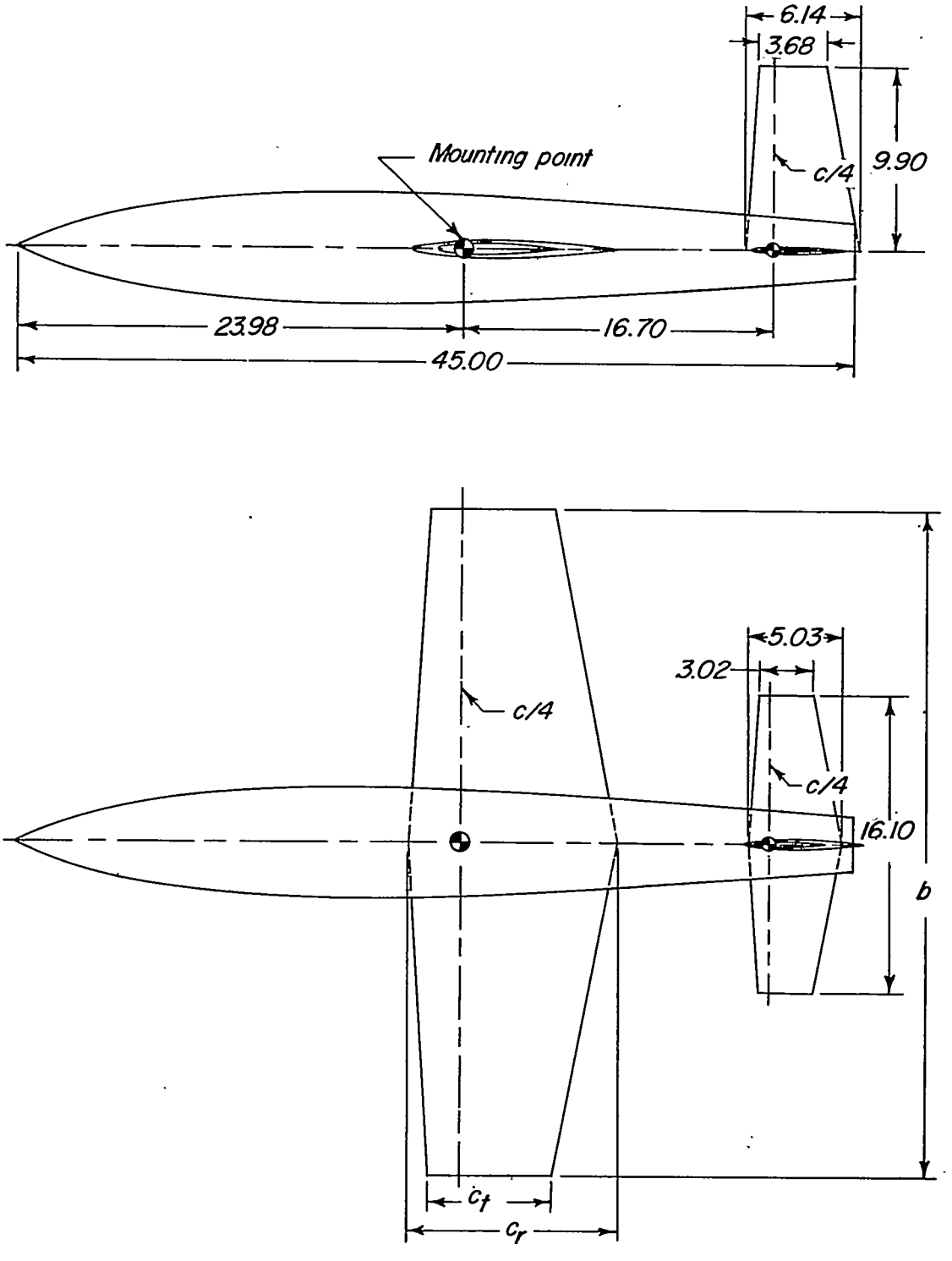

Figure 2.- General arrangement of models. All dimensions are in inches.

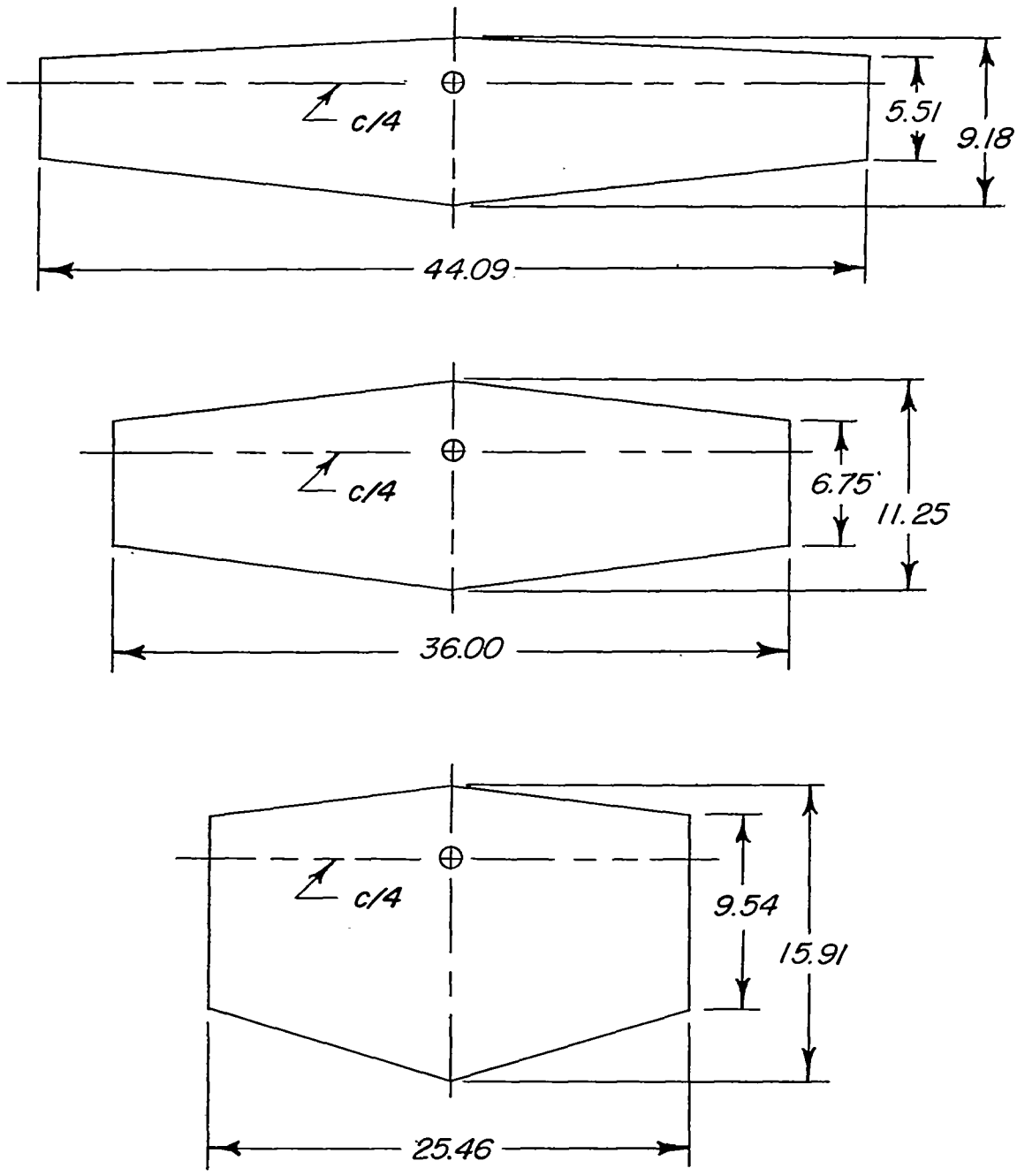

Figure 3.- Geometric characteristics of wings. All dimensions are in inches.

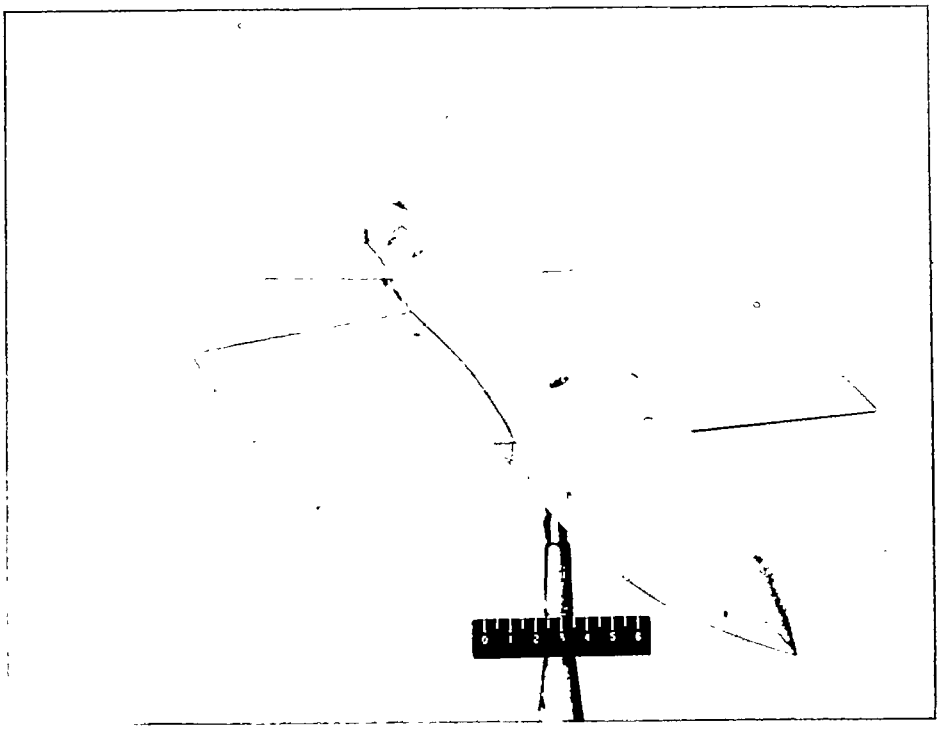

(a) Complete model with aspect-ratio-2 wing. L-82966

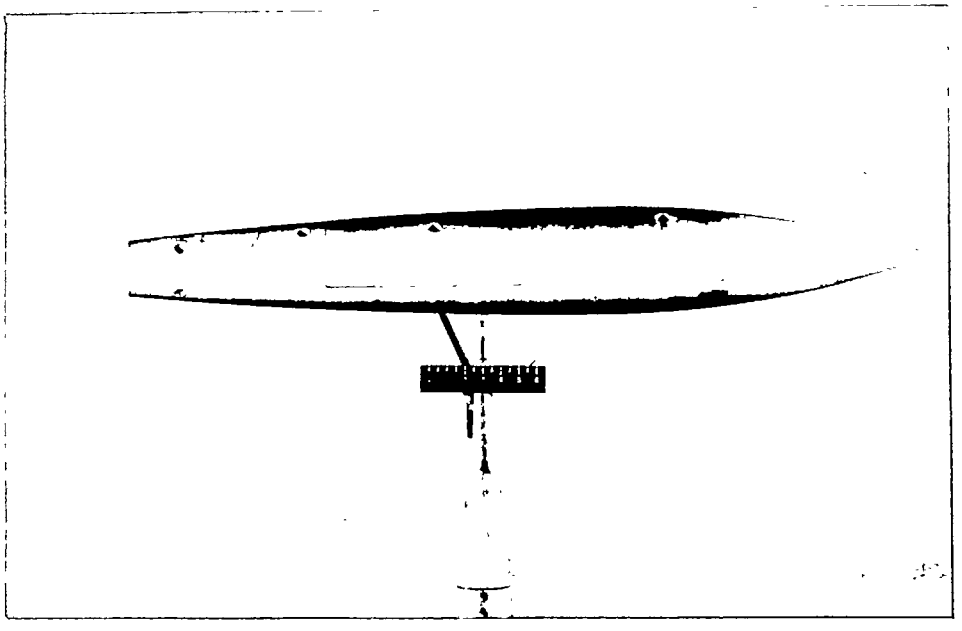

(b) Fuselage alone. L-82962

Figure 4.- Photographs of two model configurations.

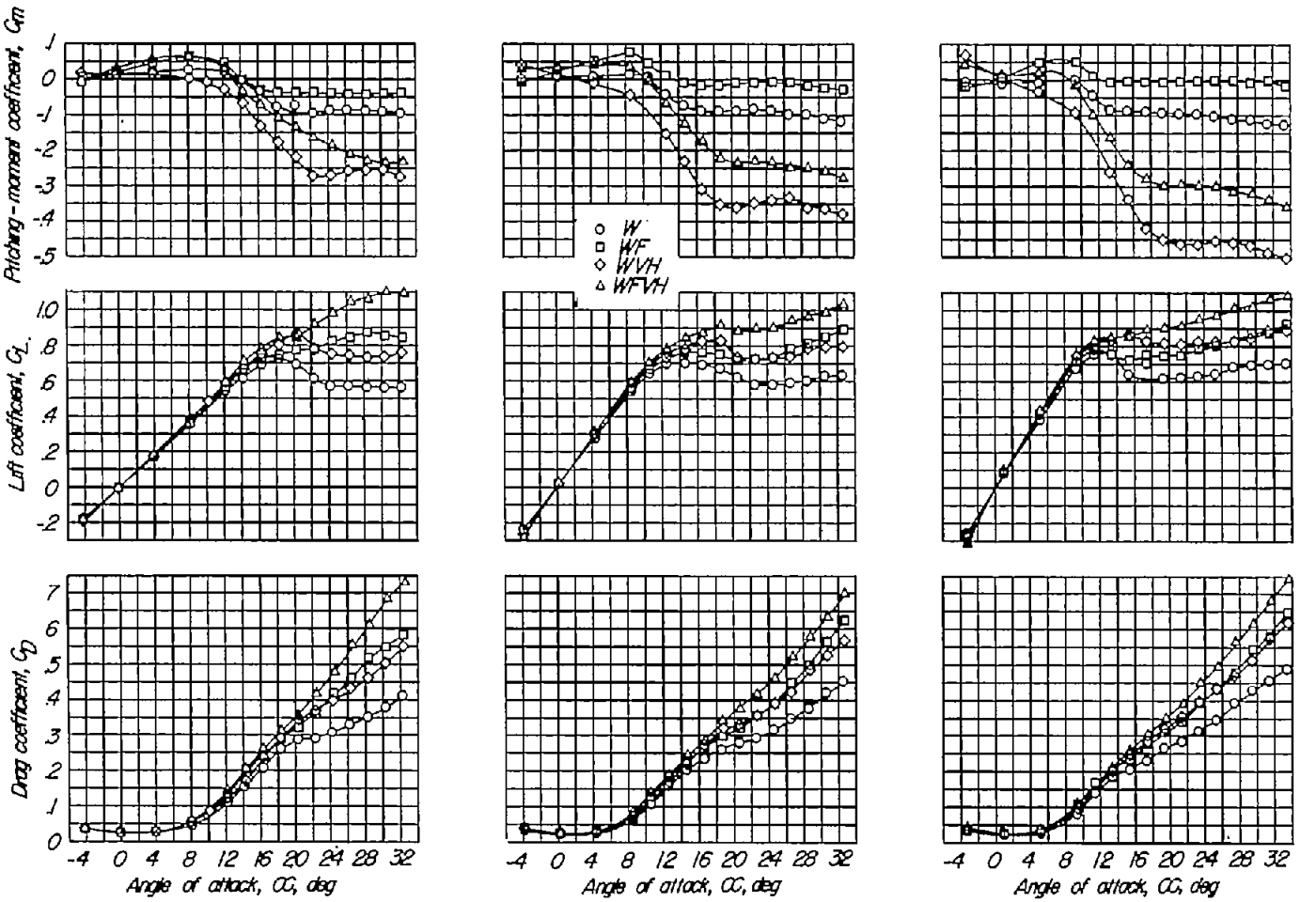

(a) Aspect-ratio-2 wing. (b) Aspect-ratio-4 wing. (c) Aspect-ratio-6 wing.

Figure 5.- Static longitudinal stability characteristics of the wing alone and in various combinations with the fuselage and tails.

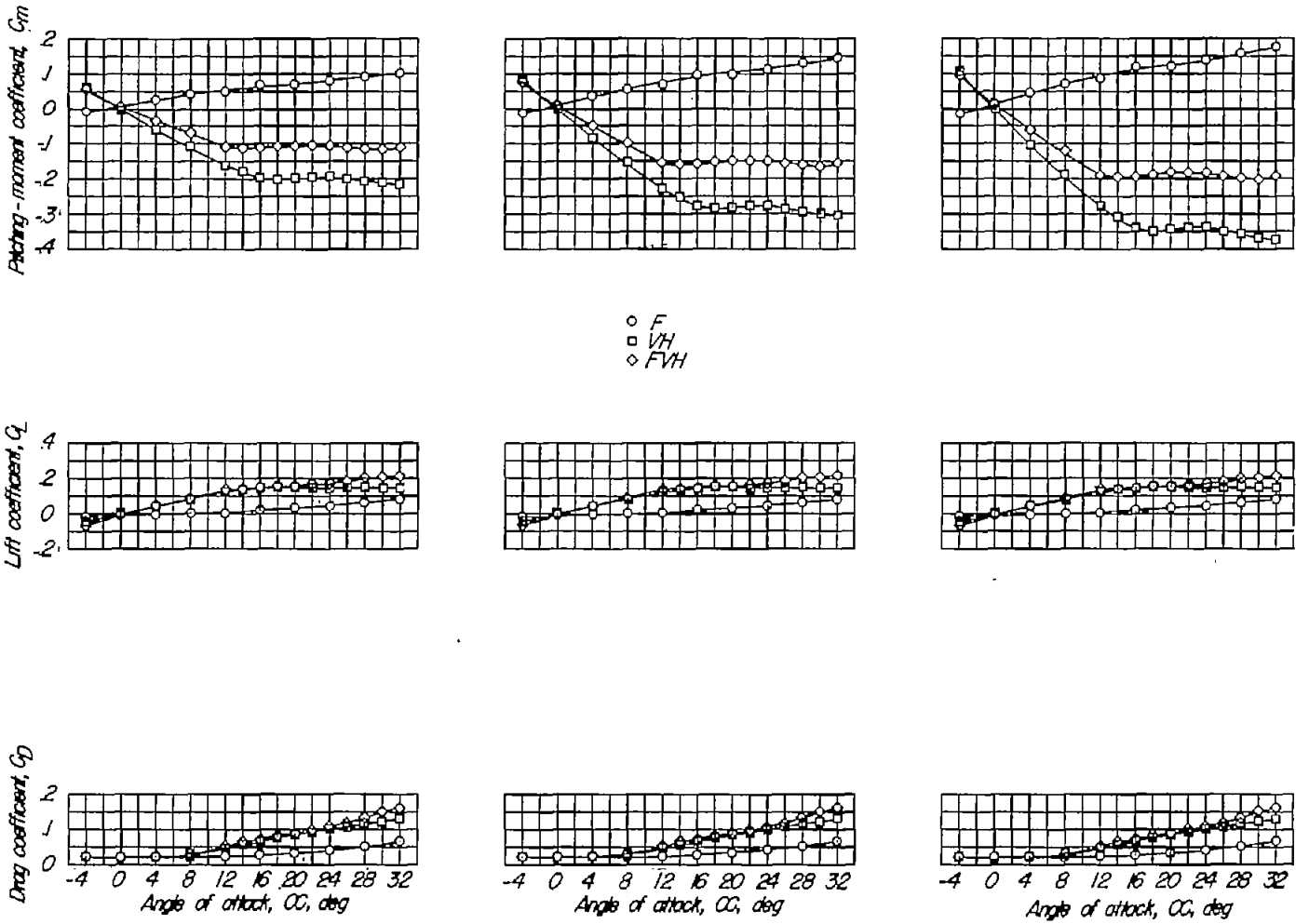

(a) Coefficients based on aspect-ratio-2 wing.

(b) Coefficients based on aspect-ratio-4 wing.

(c) Coefficients based on aspect-ratio-6 wing.

Figure 6.- Static longitudinal stability characteristics of the fuselage alone, tail alone, and fuselage-tail combination.

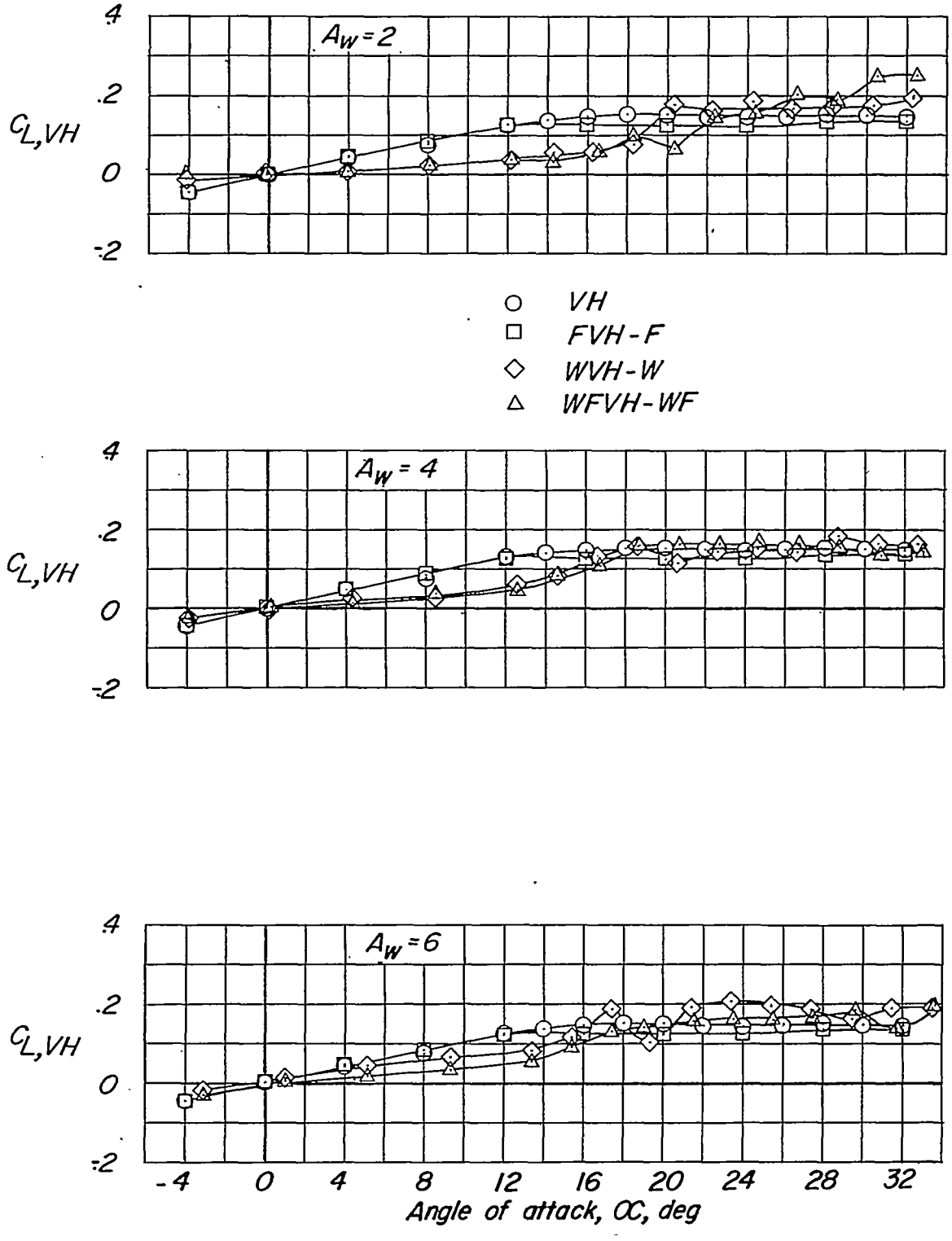

Figure 7.- Effect of the various components on the tail contribution to C_L.

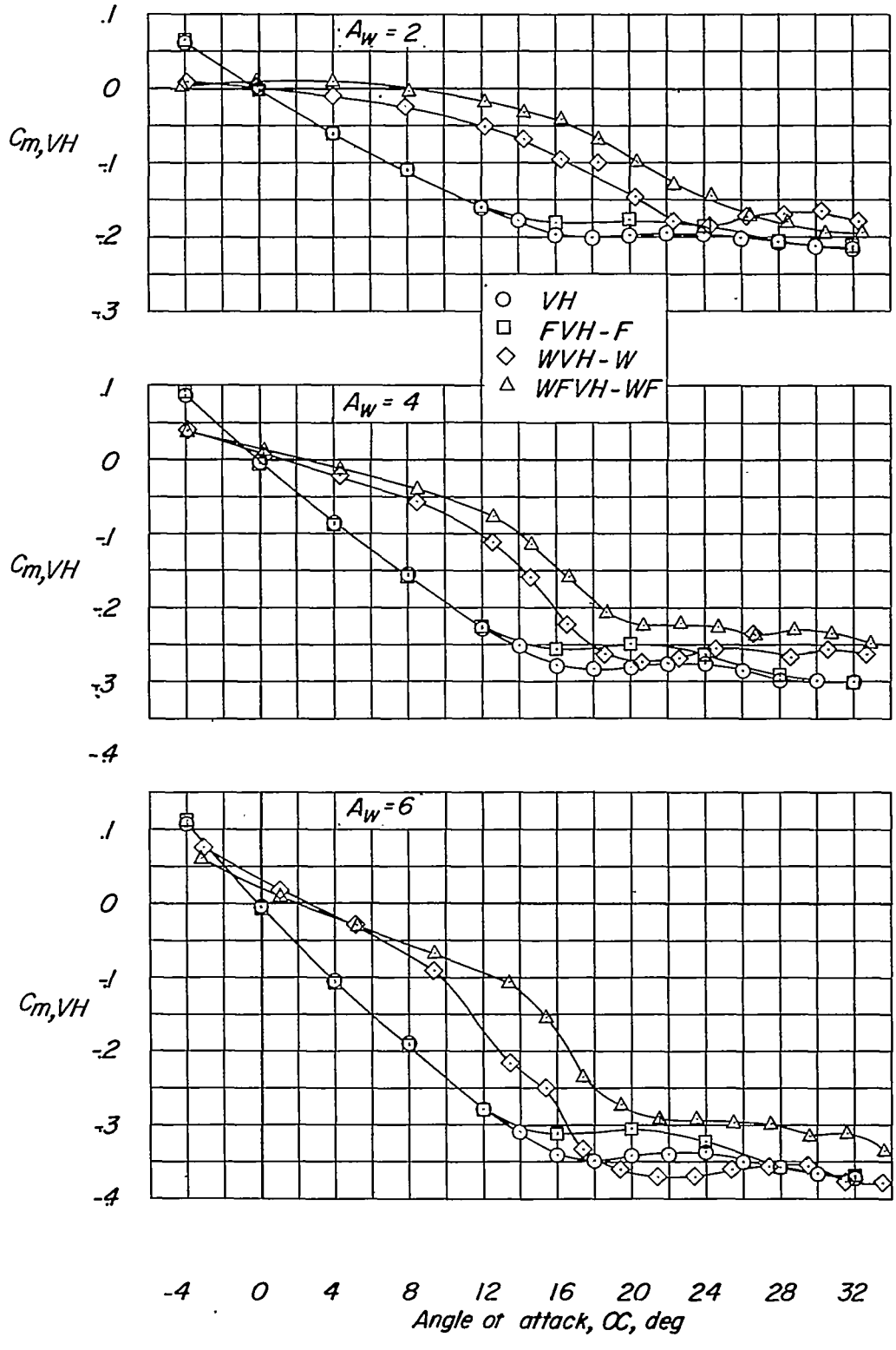

Figure 8.- Effect of the various components on the tail contribution to C_m.

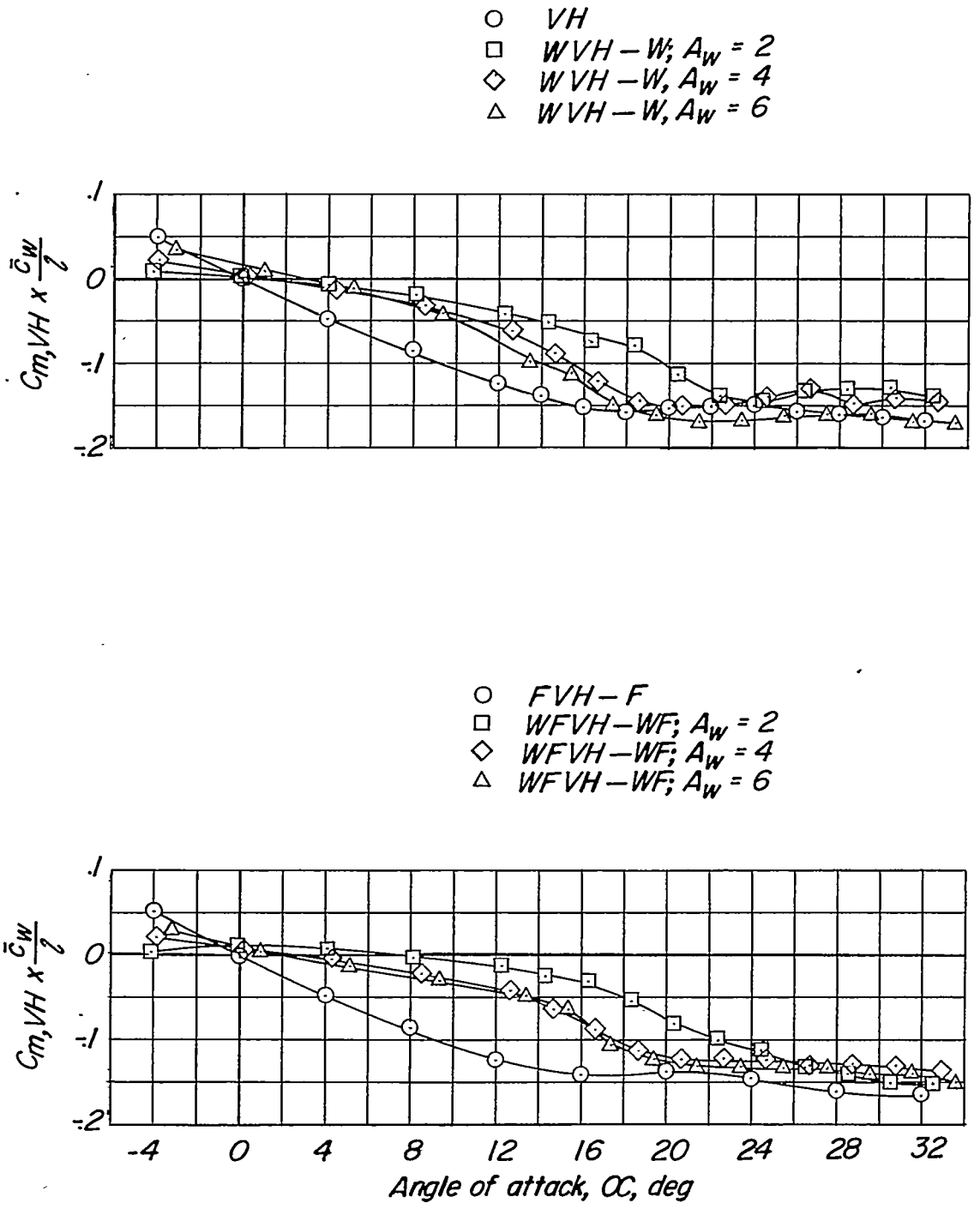

Figure 9.- Effect of wing aspect ratio on the variation of $C_{m,VH} \times \bar{c}_w/l$ with α.

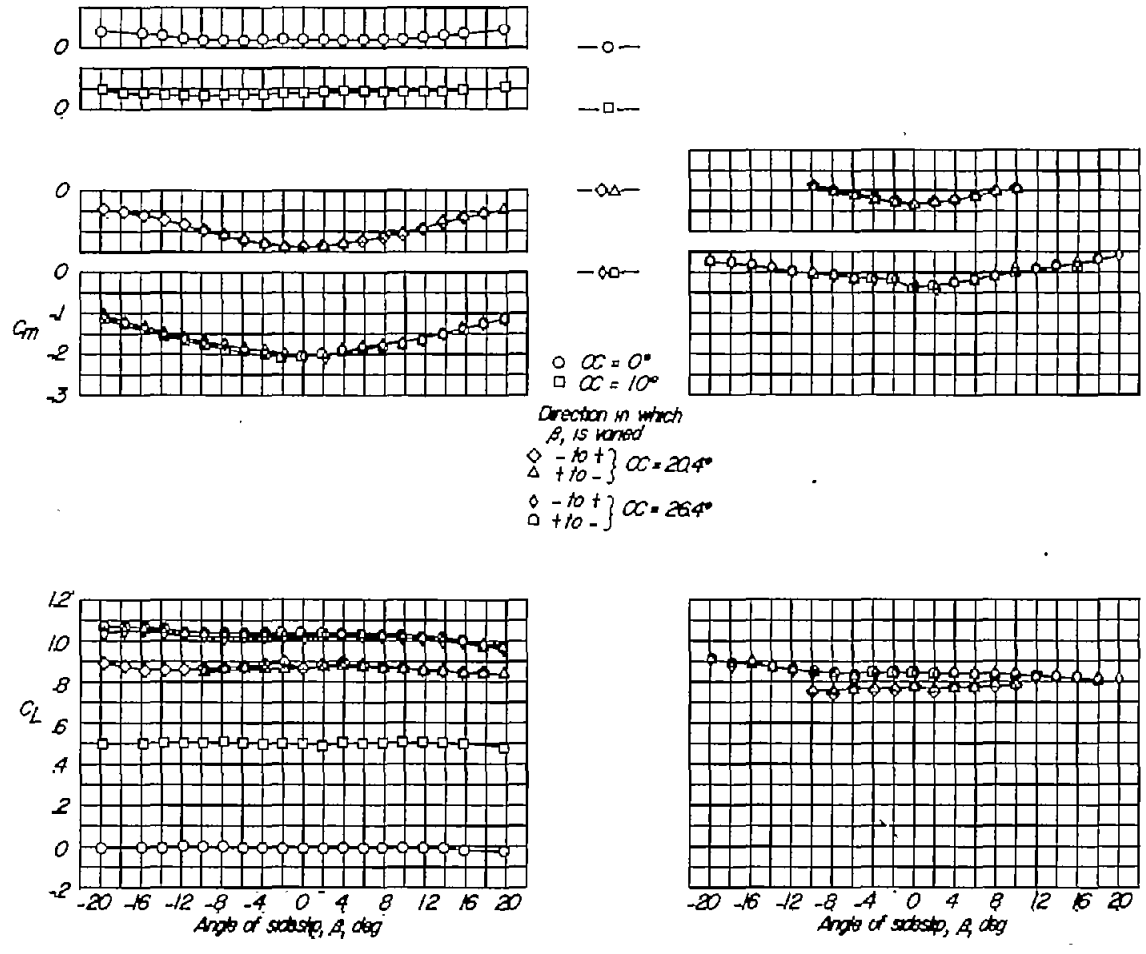

(a) Complete model.

(b) Wing-fuselage combination.

Figure 10.- Variation of C_L and C_m with β for the complete model and the wing-fuselage combination. $A_w = 2$.

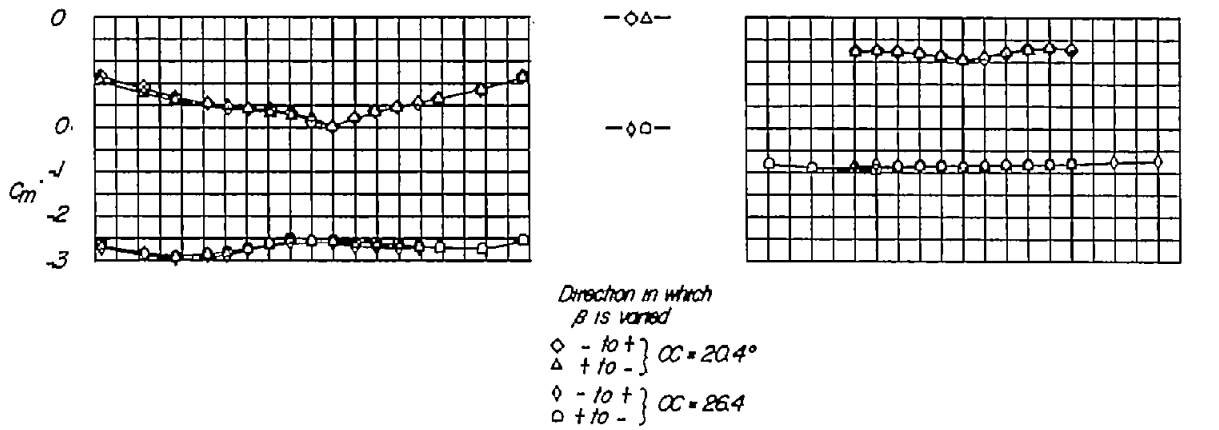

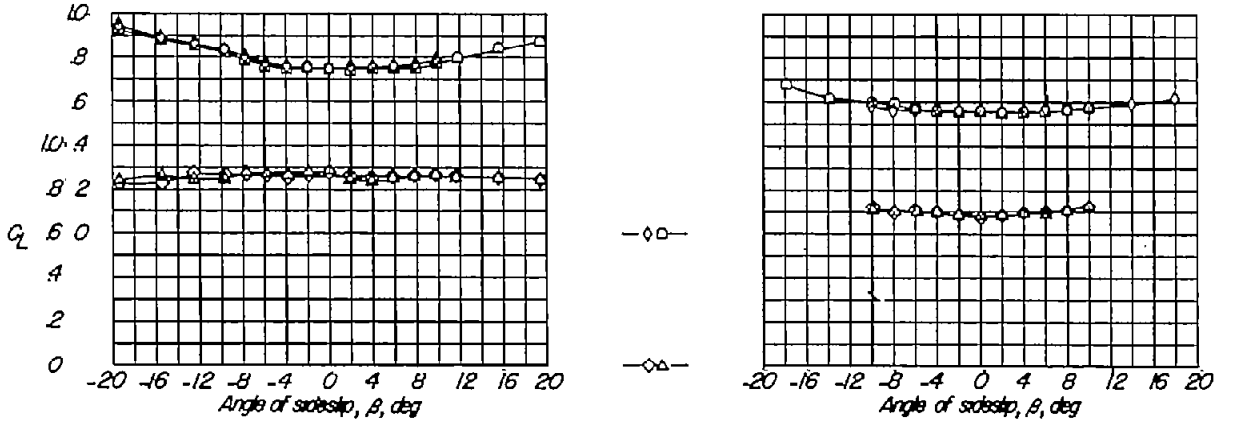

(a) Wing-tail combination.

(b) Wing alone.

Figure 11.- Variation of C_L and C_m with β for the wing-tail combination and the wing alone. $A_W = 2$.

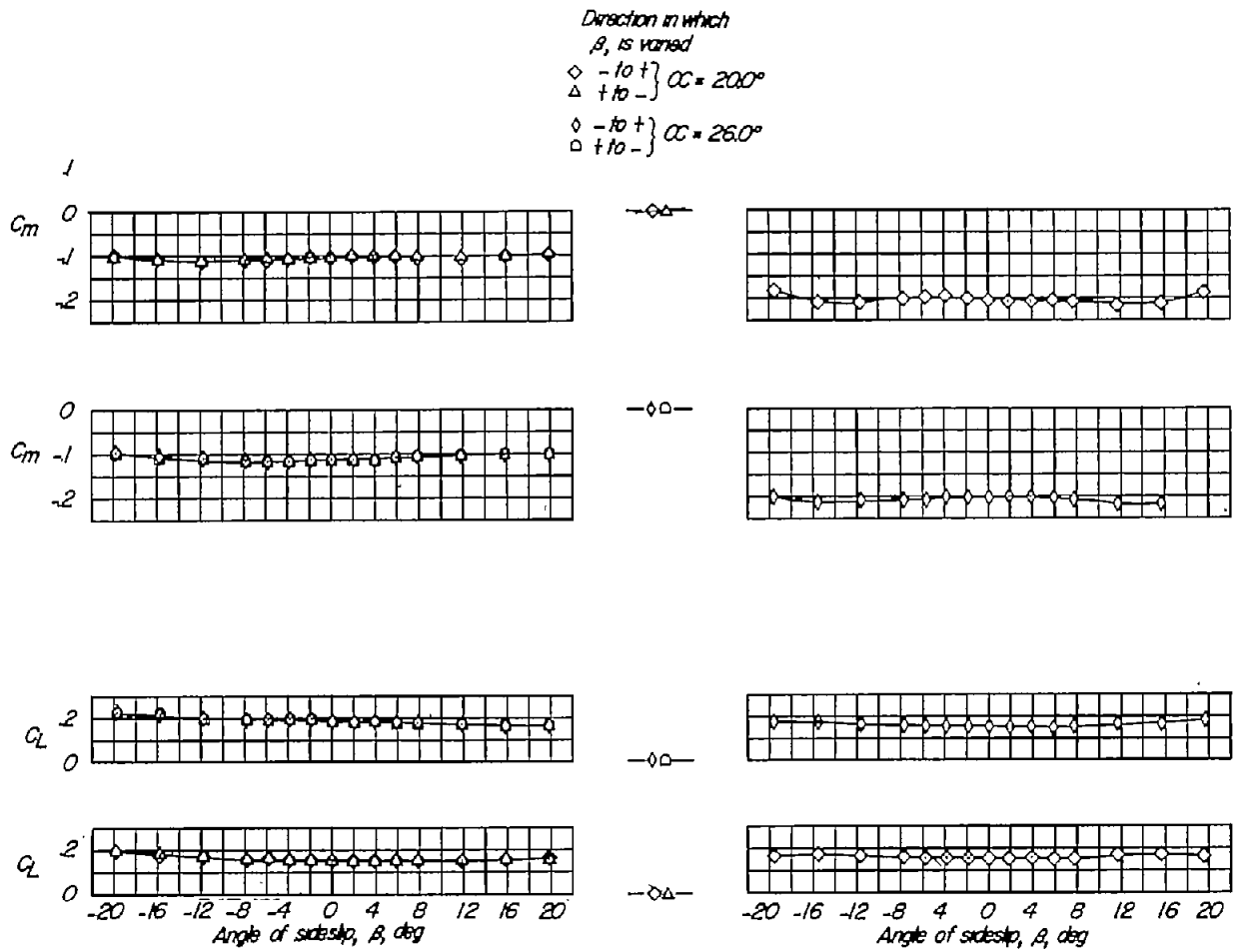

(a) Fuselage-tail combination. (b) Vertical-horizontal tail combination.

Figure 12.- Variation of C_L and C_m with β for the fuselage-tail combination and the tails alone. Coefficients are based on aspect-ratio-2 wing.

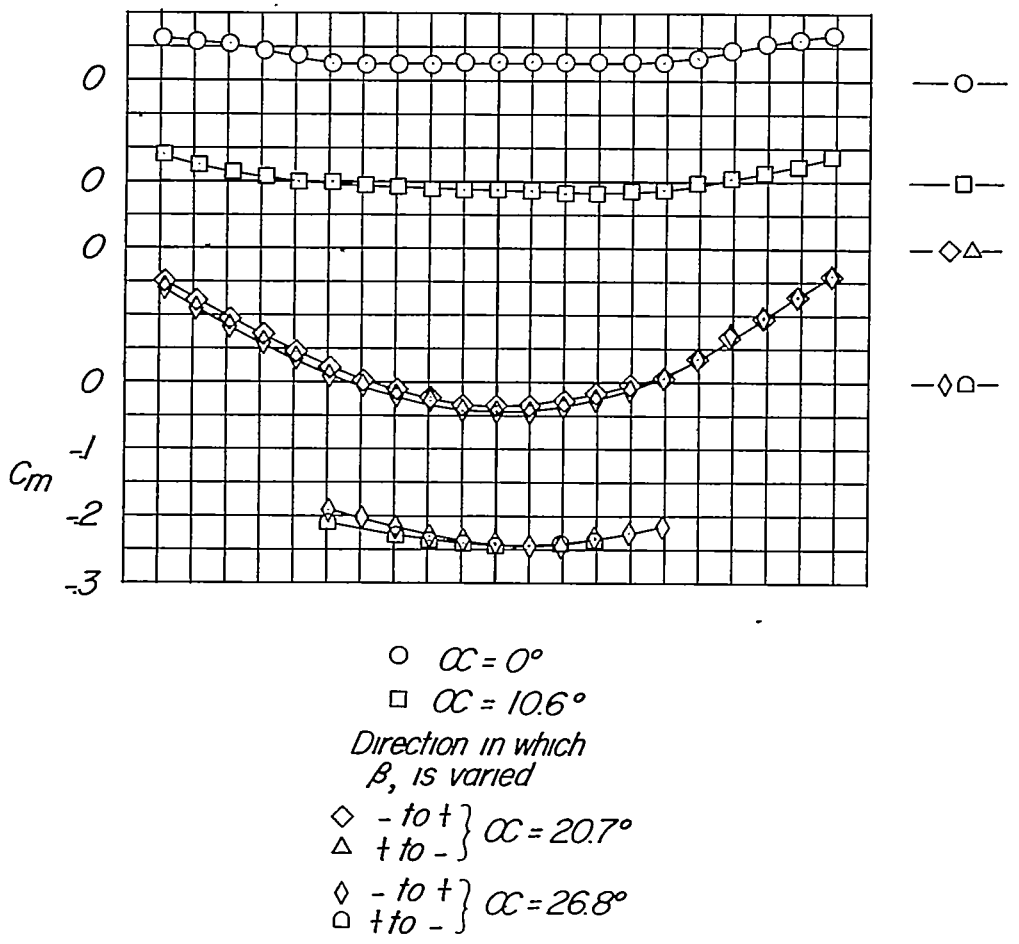

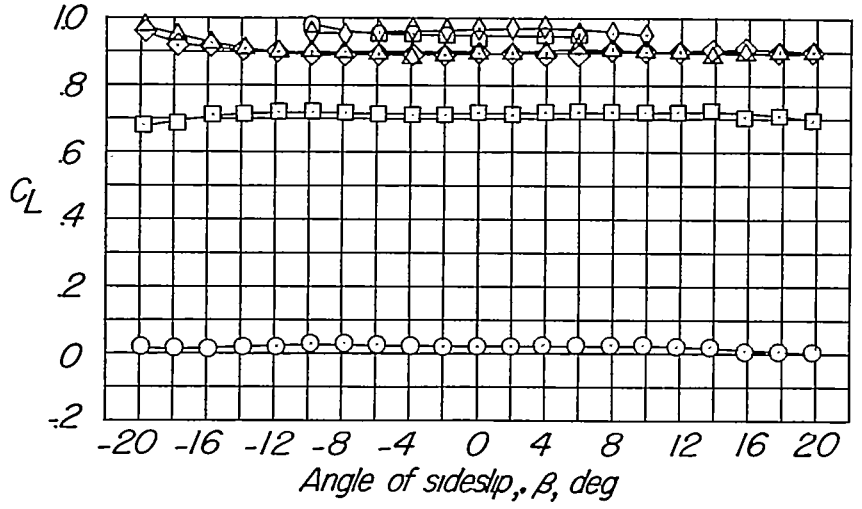

Figure 13.- Variation of C_L and C_m with β for the complete model. $A_w = 4$.

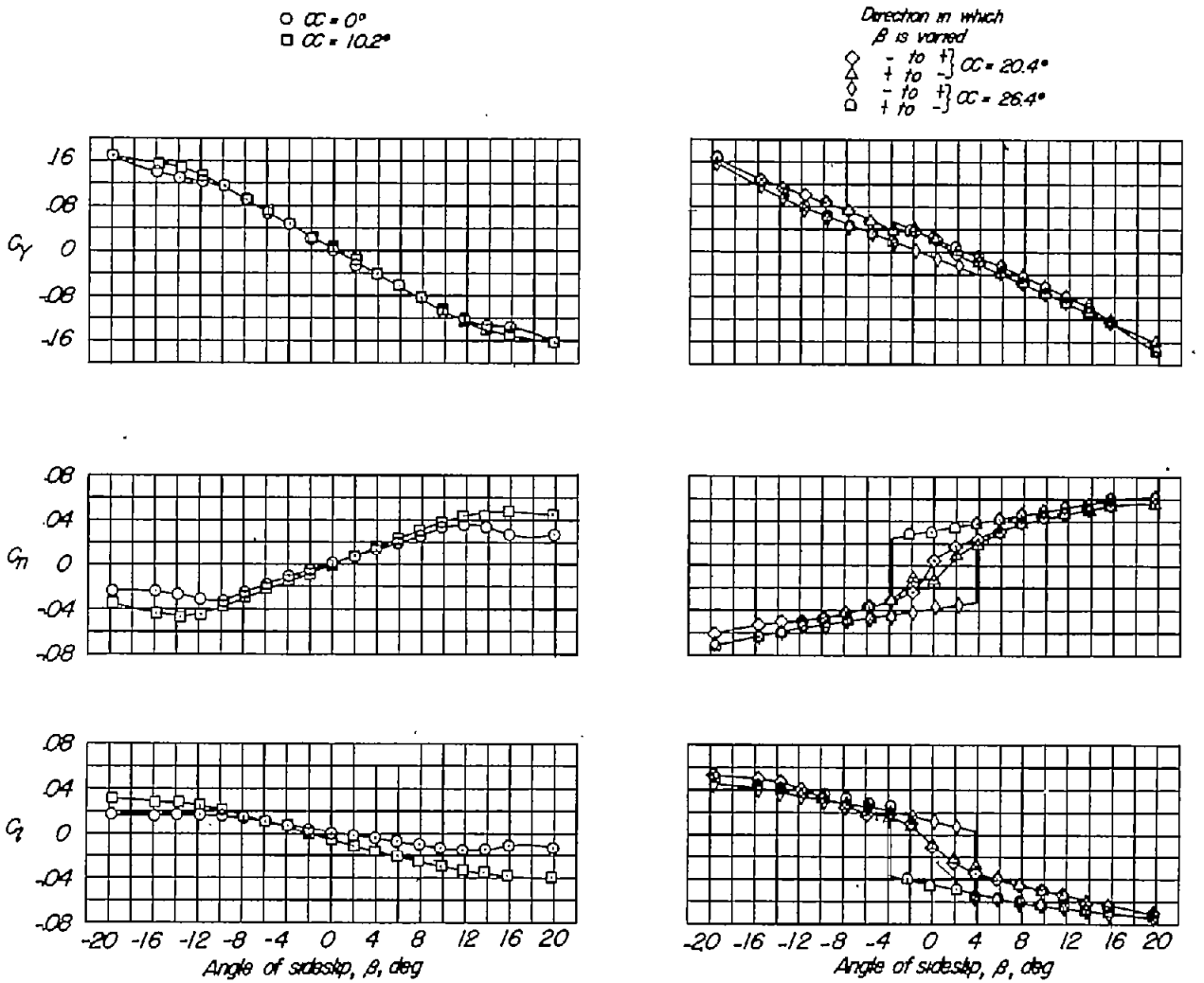

Figure 14.- Variation of C_Y, C_n, and C_l with β for the complete model. $A_W = 2$.

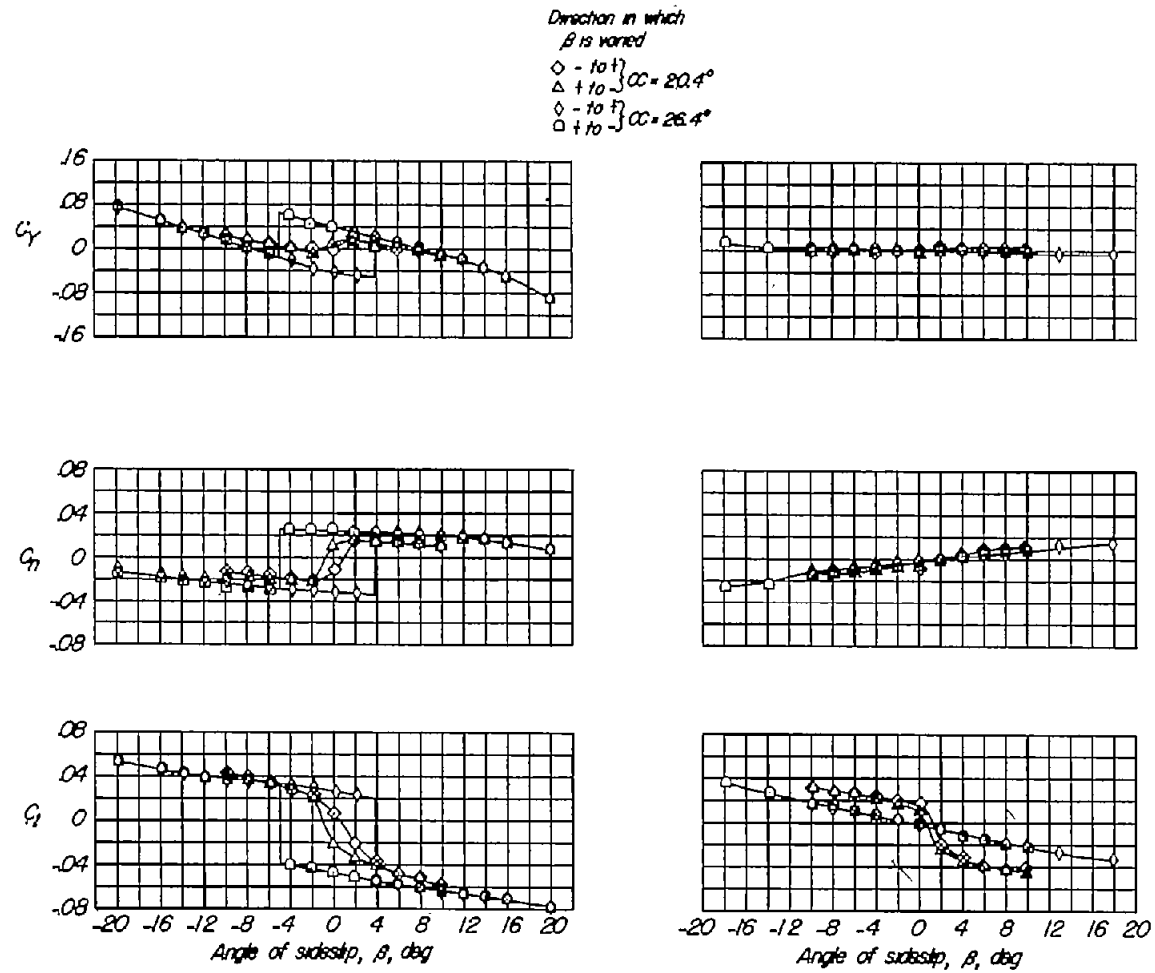

(a) Wing-fuselage combination.

(b) Wing alone.

Figure 15.- Variation of C_Y, C_n, and C_l with β for the wing-fuselage combination and the wing alone. $A_W = 2$.

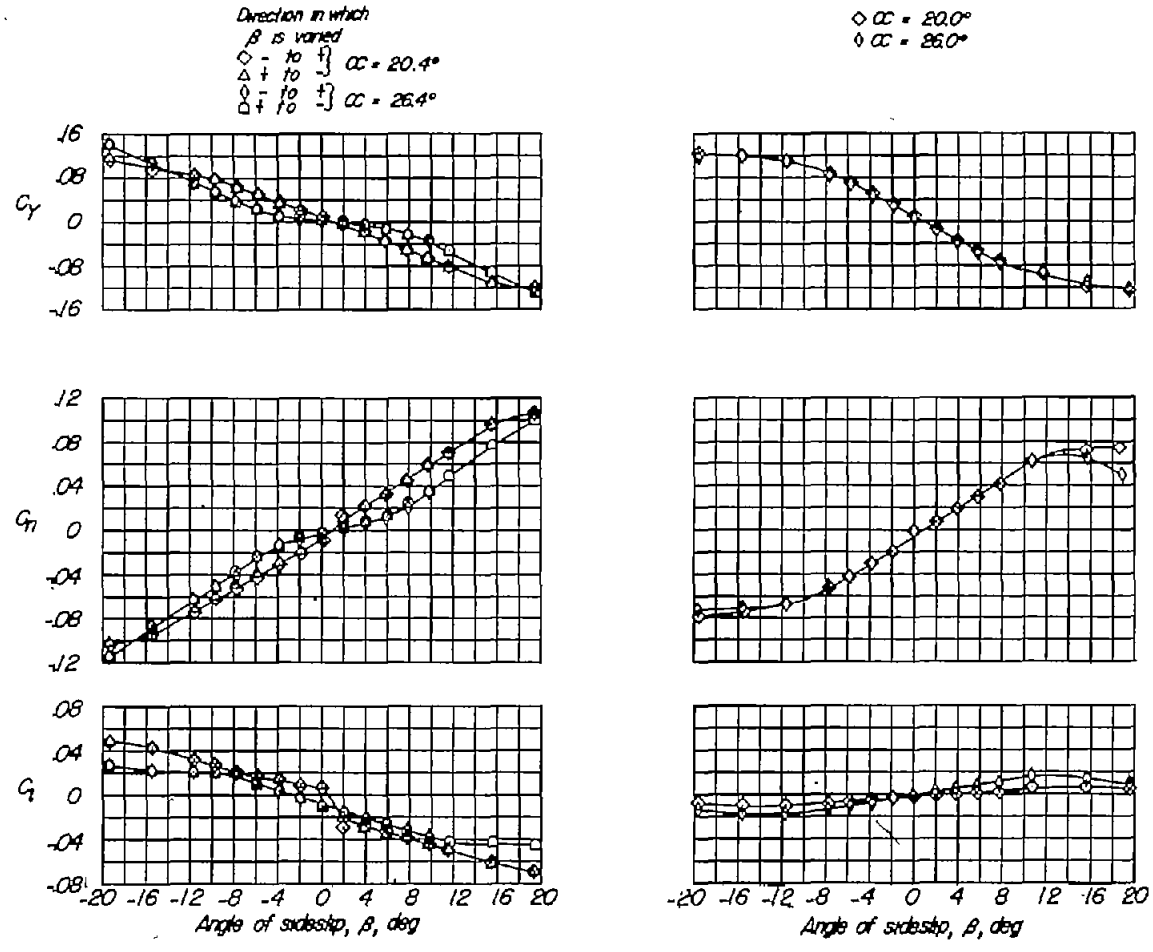

(a) Wing-tail combination.

(b) Tails alone.

Figure 16.- Variation of C_Y, C_n, and C_l with β for the wing-tail combination and the tails alone. $A_w = 2$.

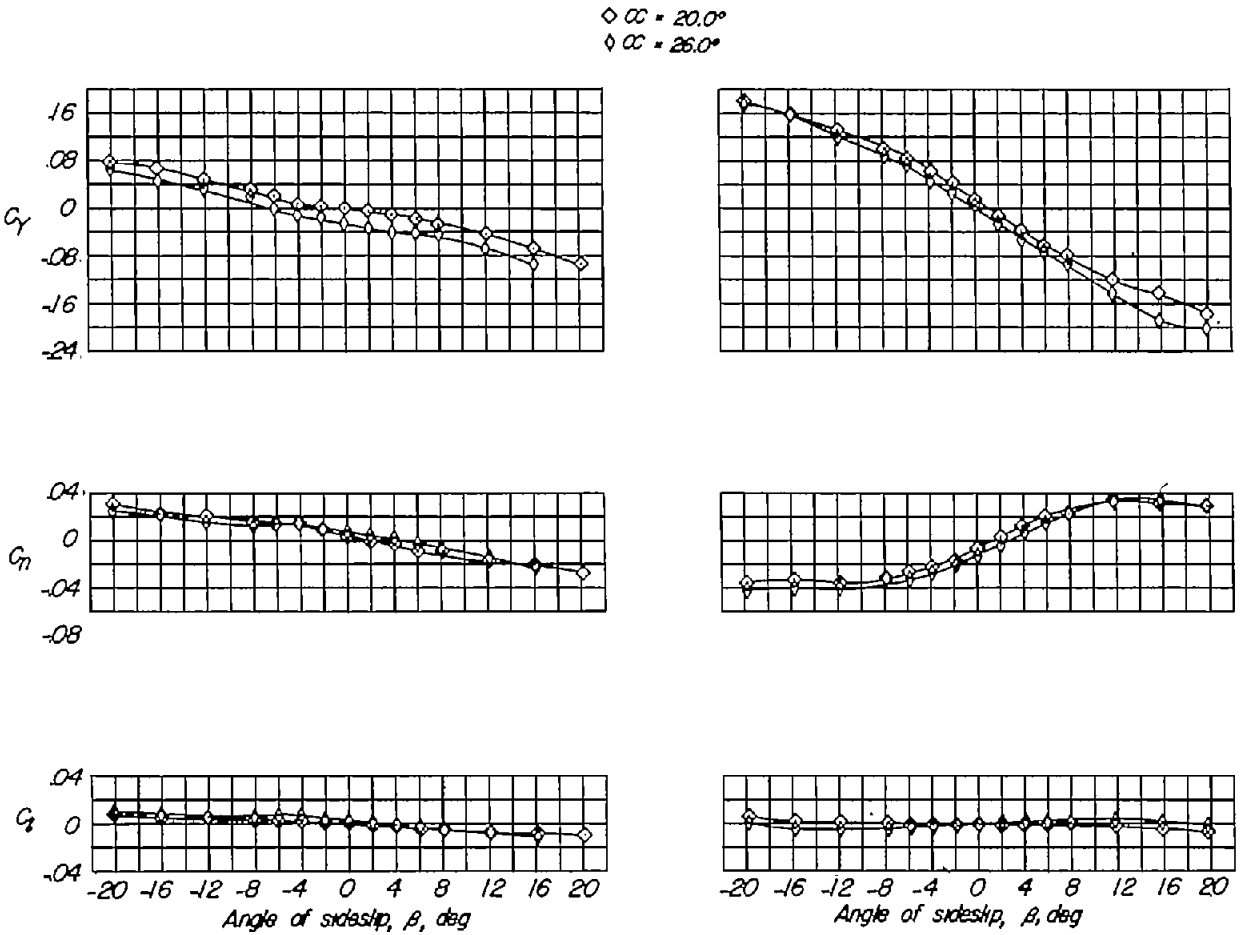

(a) Fuselage alone.

(b) Fuselage-tail combination.

Figure 17.- Variation of C_Y, C_n, and C_l with β for the fuselage alone and the fuselage-tail combination. Coefficients are based on aspect-ratio-2 wing.

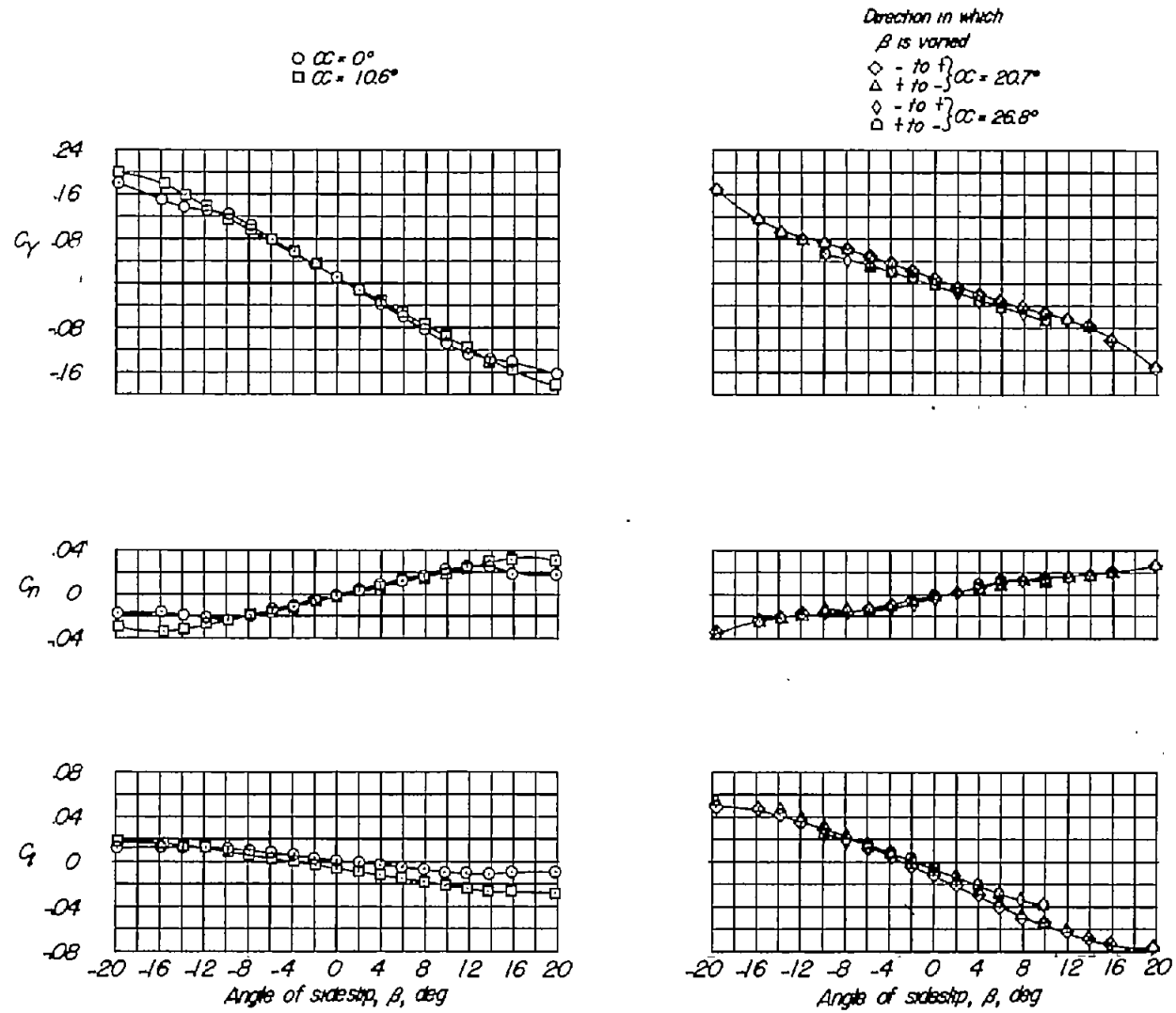

Figure 18.- Variation of C_Y, C_n, and C_l with β for the complete model. $A_W = 4$.

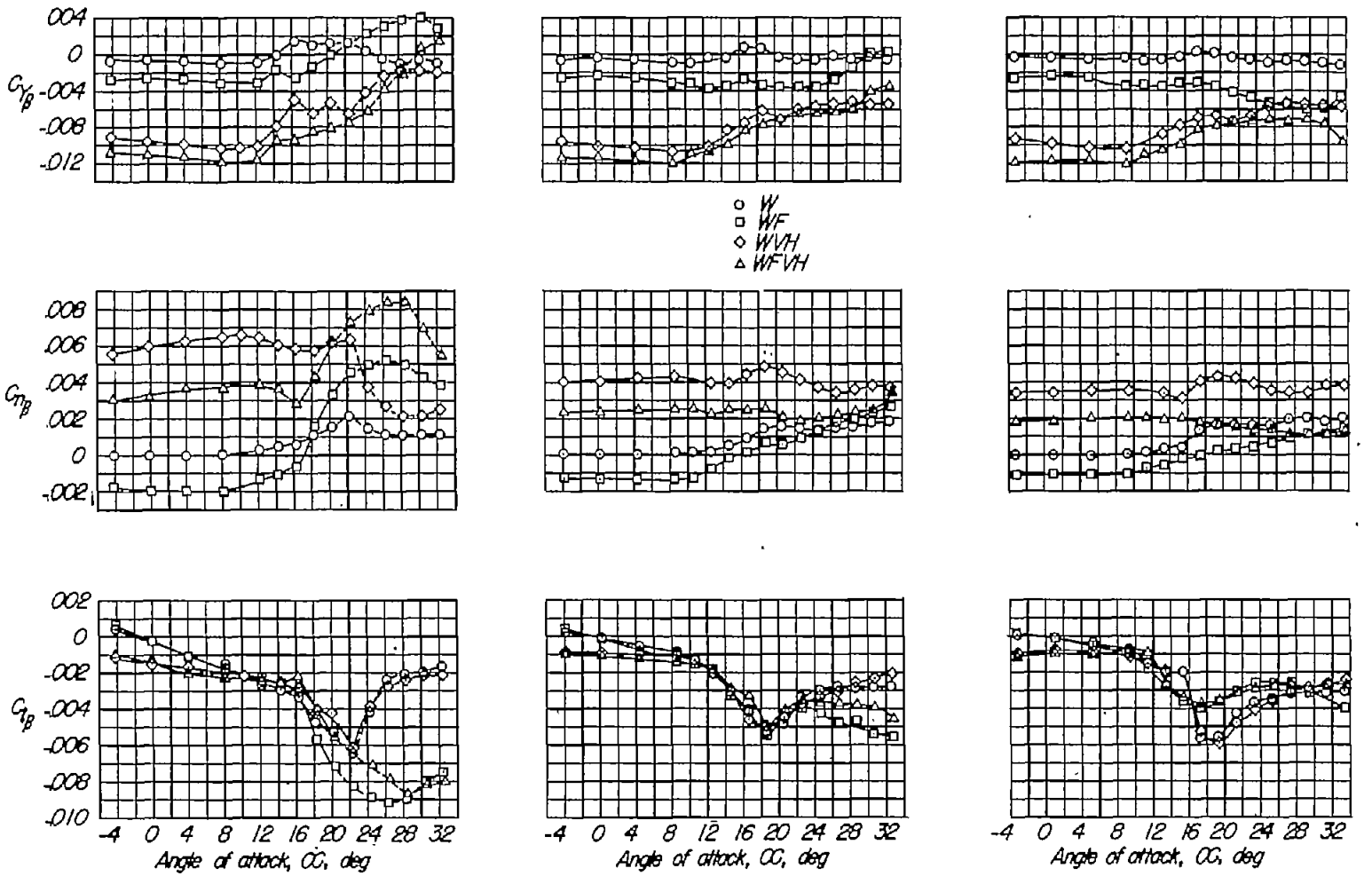

(a) Aspect-ratio-2 wing. (b) Aspect-ratio-4 wing. (c) Aspect-ratio-6 wing.

Figure 19.- Static lateral stability characteristics of the wing alone and in various combinations with the fuselage and tails.

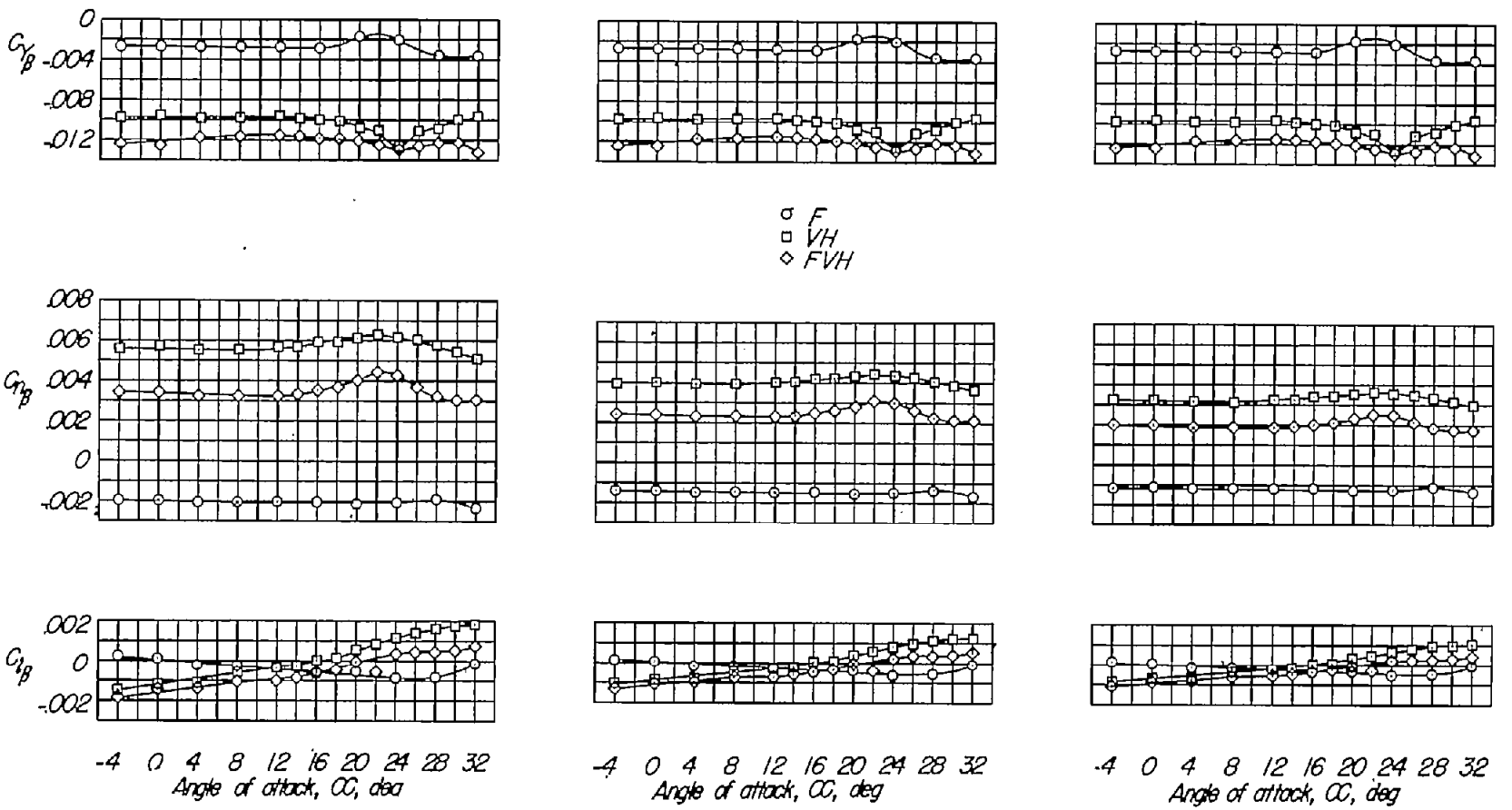

(a) Coefficients based on aspect-ratio-2 wing.

(b) Coefficients based on aspect-ratio-4 wing.

(c) Coefficients based on aspect-ratio-6 wing.

Figure 20.- Static lateral stability characteristics of the fuselage alone, tails alone, and the fuselage-tail combination.

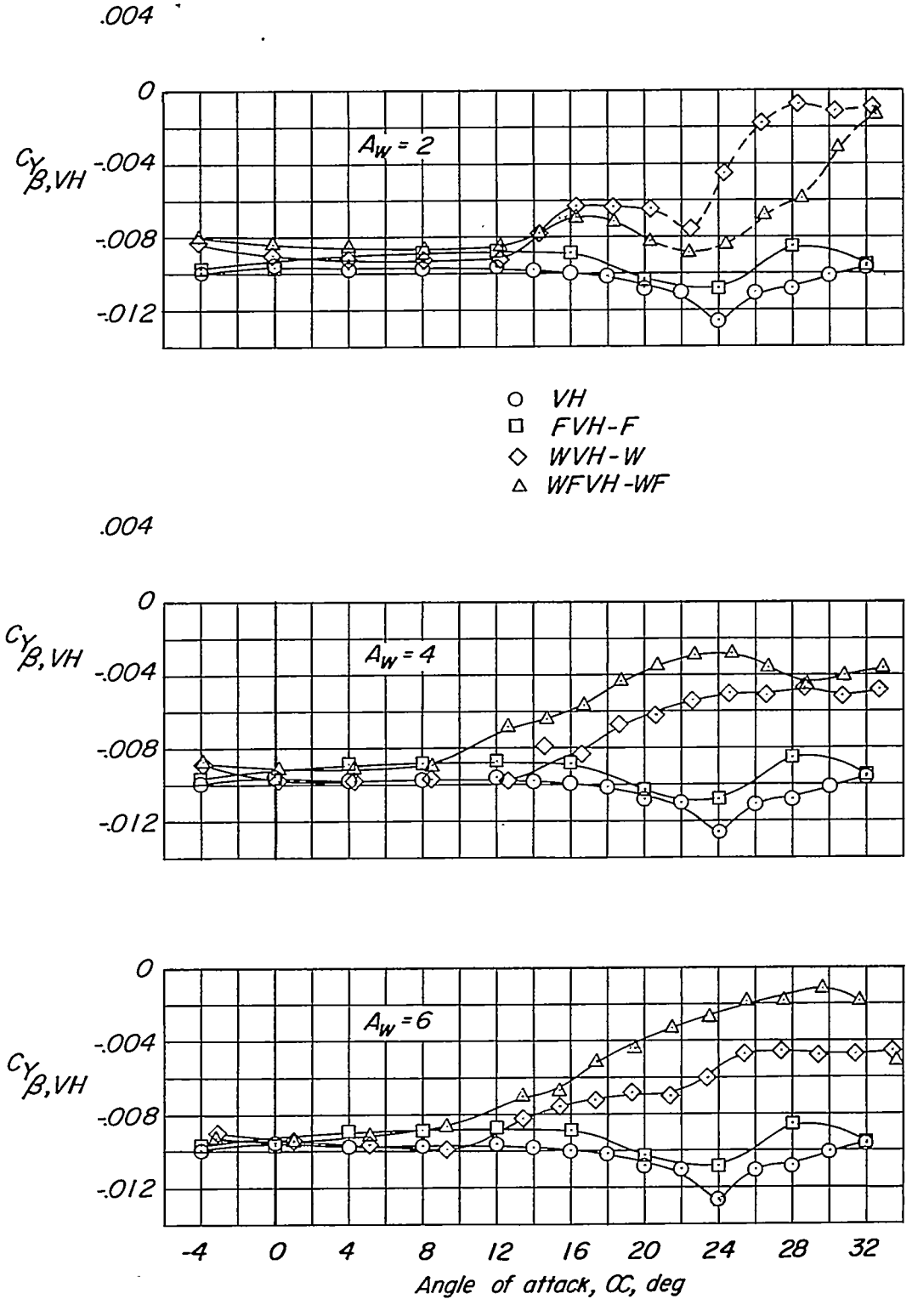

Figure 21.- Effect of the various components on the tail contribution to C_{Y_β}.

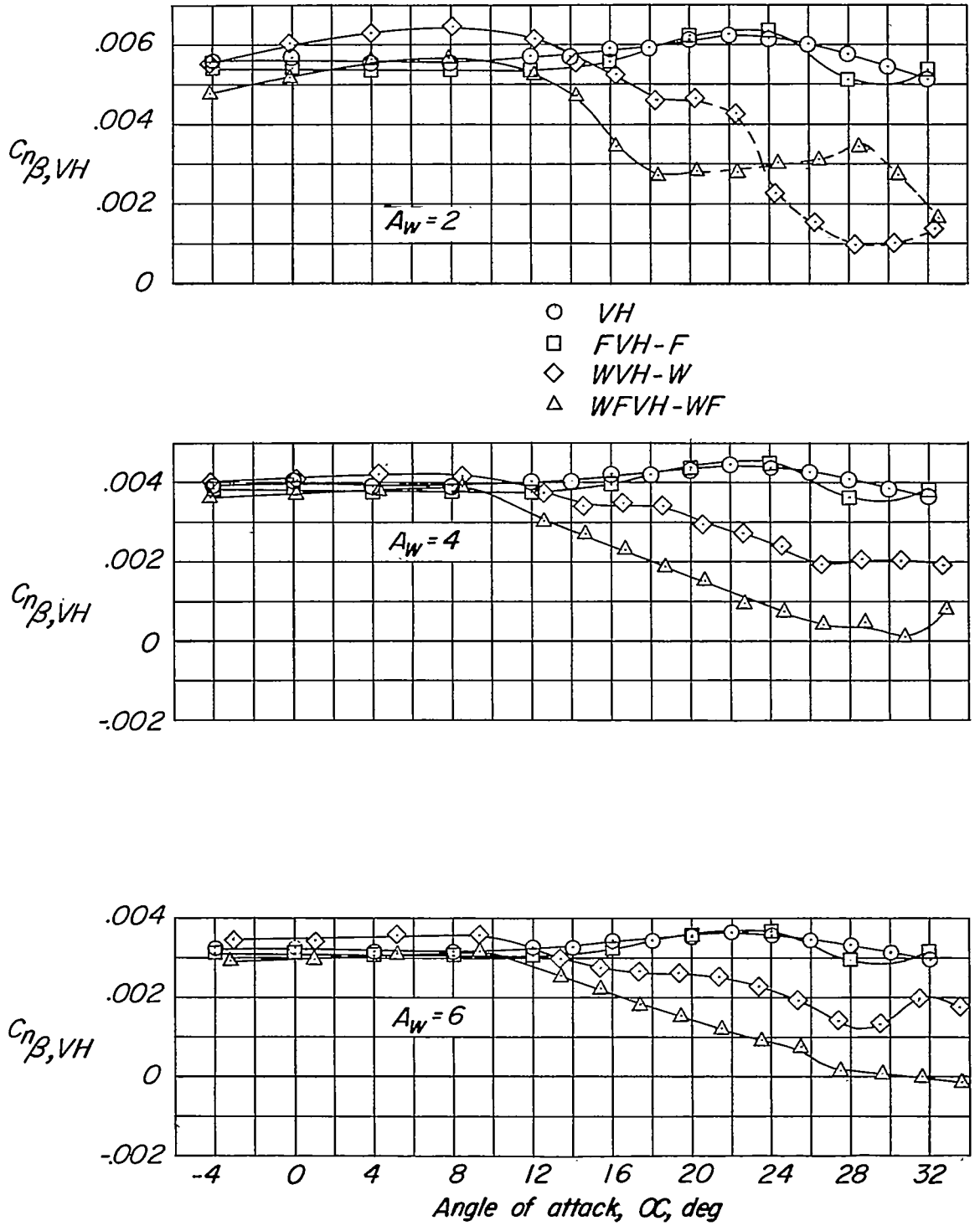

Figure 22.- Effect of the various components on the tail contribution to C_{n_β}.

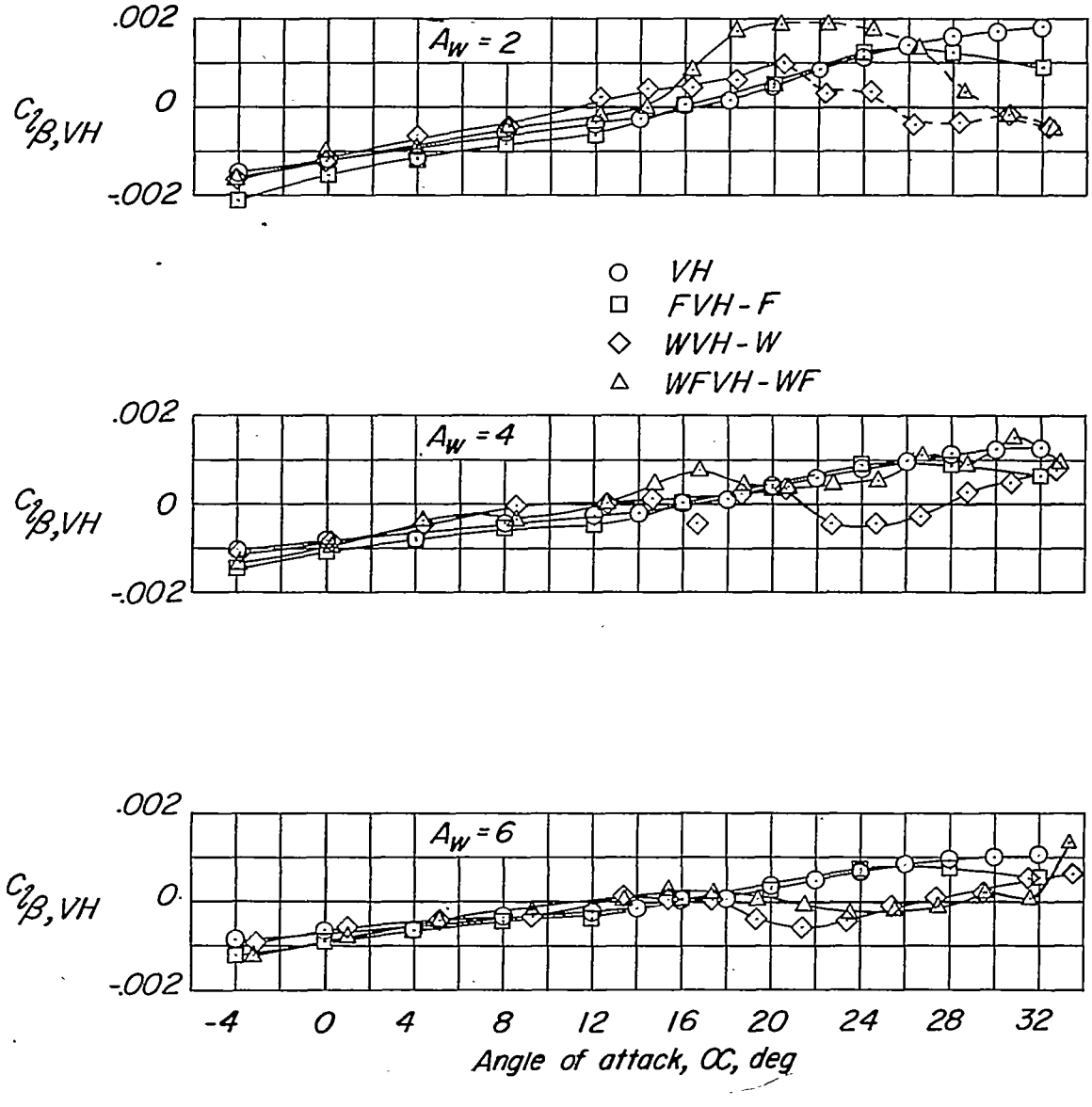

Figure 23.- Effect of the various components on the tail contribution to C_{l_β}.

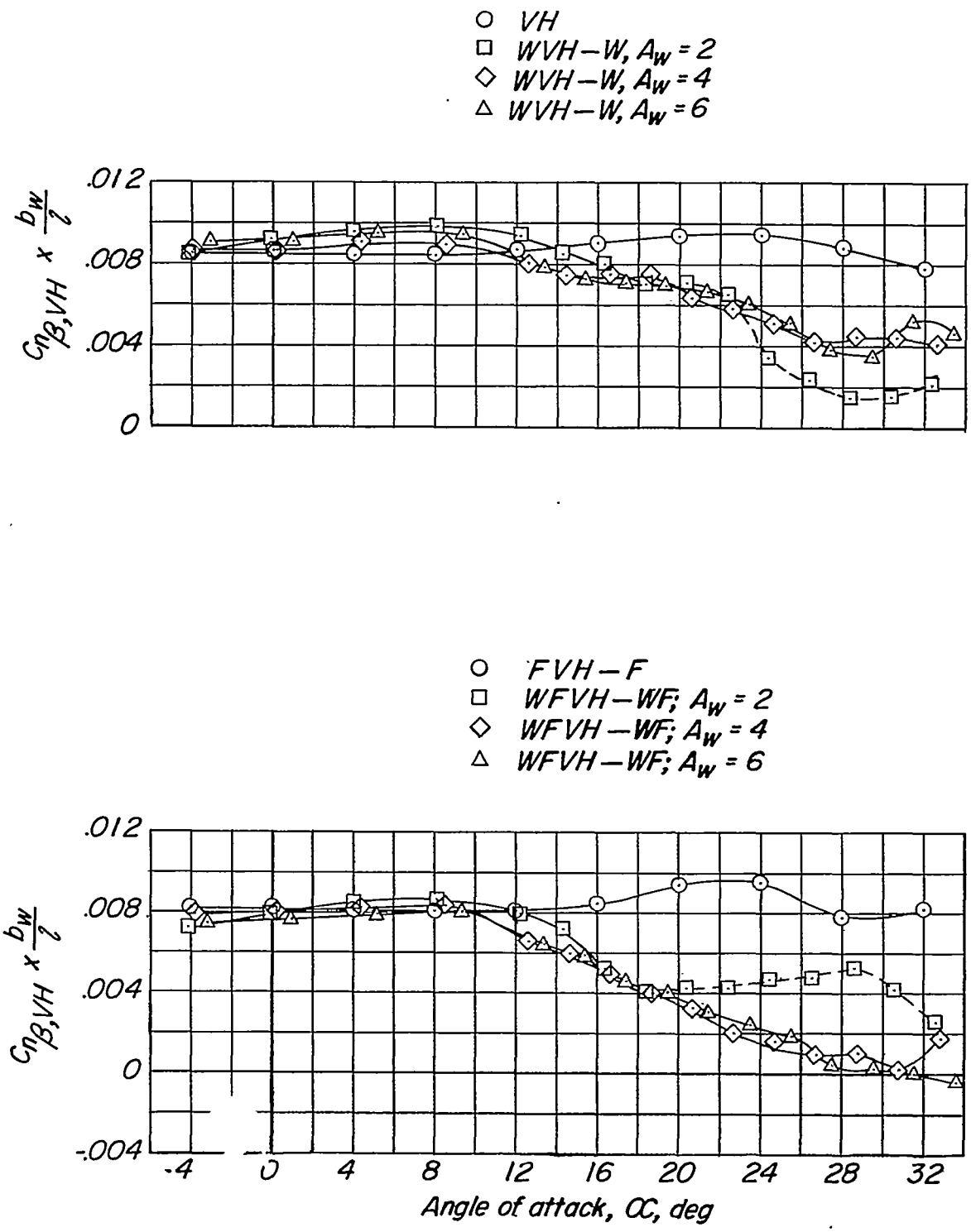

Figure 24.- Effect of wing aspect ratio on the variation of $C_{n_{\beta,VH}} \times b_W/l$ with α.